Measurements of OH and HO_2 radical concentrations and photolysis frequencies during BERLIOZ

Frank Holland, Andreas Hofzumahaus, Jürgen Schäfer, Alexander Kraus,[1] and Hans-Werner Pätz[2]

Institut für Chemie und Dynamik der Geosphäre II: Troposphäre, Forschungszentrum Jülich, Jülich, Germany

Received 15 October 2001; revised 13 February 2002; accepted 15 February 2002; published 3 January 2003.

[1] This paper presents the measurements of OH and HO_2 radical concentrations as well as photolysis frequencies of different molecules during the Berliner Ozone (BERLIOZ) field experiment in July/August 1998 at the rural site Pabstthum about 50 km NW of Berlin. Radical concentrations were measured using laser-induced fluorescence (LIF) spectroscopy, while filter radiometers and a scanning spectroradiometer were used to obtain photolysis frequencies. The radical data set covers the time period from 20 July to 6 August and consists of more than 6000 simultaneous measurements of OH and HO_2 with a typical time resolution of about 90 s. The maximum OH and HO_2 daytime concentrations were 8×10^6 and 8×10^8 cm^{-3}, respectively. While nighttime values of OH were usually below the detection limit of our instrument (3.5×10^5 cm^{-3}), HO_2 did show significant concentrations throughout most of the nights (on average 3×10^7 cm^{-3}). The OH concentration was mainly controlled by solar UV radiation and showed a high linear correlation with $J(O^1D)$. A deviation from this general behavior was observed around dawn and dusk, when OH concentrations well above the detection limit were observed, although $J(O^1D)$ was essentially zero. A comparison with data sets from previous campaigns revealed that even though the linear correlation is found in other environments as well the slope $[OH]/J(O^1D)$ differs significantly. The diurnal cycles of HO_2 were less dependent on the solar actinic flux but were predominantly influenced by NO. During episodes of high NO, HO_2 remained below the detection limit (1×10^7 cm^{-3}) but started to rise rapidly as soon as NO started to decrease. *INDEX TERMS:* 0322 Atmospheric Composition and Structure: Constituent sources and sinks; 0345 Atmospheric Composition and Structure: Pollution—urban and regional (0305); 0365 Atmospheric Composition and Structure: Troposphere—composition and chemistry; 0394 Atmospheric Composition and Structure: Instruments and techniques; *KEYWORDS:* laser-induced fluorescence, filter radiometer, spectroradiometer, urban plume, photochemistry, correlation

Citation: Holland, F., A. Hofzumahaus, J. Schäfer, A. Kraus, and H. W. Pätz, Measurements of OH and HO_2 radical concentrations and photolysis frequencies during BERLIOZ, *J. Geophys. Res.*, *108*(D4), 8246, doi:10.1029/2001JD001393, 2003.

1. Introduction

[2] The hydroxyl radical (OH) has long been recognized to be the most important oxidizing agent in the troposphere [e.g., *Levy*, 1972; *Logan et al.*, 1981; *Ehhalt*, 1999b]. The decomposition of most trace gases is initiated by their gas-phase reaction with OH. In many instances this reaction is the rate-limiting step in a chain of reactions finally leading to products, which are easily removed from the atmosphere by uptake on water droplets or dry deposition. Thus, the atmospheric life times and concentrations of many species are controlled by the concentration of OH radicals. Beside its high reactivity the importance of OH for the self-cleansing capability of the atmosphere is largely due to the fact that many of the OH reactions result in the production of a hydroperoxy radical (HO_2), which in turn can react with other trace gas molecules to yield OH again. Thus, one OH radical can initiate the degradation of several trace gas molecules before it is finally removed from the atmosphere. Since OH and HO_2 are interconverted within seconds they are often summarized as HO_x family.

[3] In the clean atmosphere the most important source of OH is the photolysis of ozone at wavelengths shorter than 340 nm yielding an excited oxygen atom (O^1D), which subsequently reacts with ambient water vapor to form two OH radicals:

$$O_3 + h\nu \longrightarrow O(^1D) + O_2 (\lambda \leq 340\ nm) \qquad (1)$$

[1] Now at Grünenthal GmbH, Aachen, Germany.

[2] Now at ICG 2: Institut für Chemie der Belasteten Atmosphäre, Forschungszentrum Jülich, Jülich, Germany.

0148-0227/03/2001JD001393

$$H_2O + O(^1D) \longrightarrow 2OH \quad (2)$$

In the more polluted atmosphere other photolytic processes may become important as well. The photolysis of nitrous acid (HONO), a compound which may accumulate during nighttime in the presence of high NO_2 levels, is considered to be a dominant OH source in the early morning hours when the high zenith angle of the Sun does not allow the short-wavelength UV-B radiation to efficiently penetrate the atmosphere. Also the photolysis of hydrogen peroxide may contribute to the OH production:

$$HONO + h\nu \longrightarrow OH + NO(\lambda \leq 400\ nm) \quad (3)$$

$$H_2O_2 + h\nu \longrightarrow OH + OH(\lambda \leq 400\ nm) \quad (4)$$

The photolysis of aldehydes lead, in part, to the formation of HO_2 radicals:

$$HCHO + h\nu \longrightarrow H + HCO(\lambda \leq 335\ nm) \quad (5)$$

$$HCHO + h\nu \longrightarrow H_2 + CO(\lambda \leq 360\ nm) \quad (6)$$

$$CH_3CHO + h\nu \longrightarrow CH_3 + HCO(\lambda \leq 330\ nm) \quad (7)$$

$$HCO + O_2 \longrightarrow HO_2 + CO \quad (8)$$

$$H + O_2 + M \longrightarrow HO_2 + M \quad (9)$$

The reaction of HO_2 with NO is an important secondary source of OH and an essential step in the photochemical production of tropospheric ozone:

$$HO_2 + NO \longrightarrow OH + NO_2 \quad (10)$$

$$NO_2 + h\nu \longrightarrow NO + O(\lambda \leq 420\ nm) \quad (11)$$

$$O + O_2 + M \longrightarrow O_3 + M \quad (12)$$

Beside these photolytic sources there are some chemical reactions, which are capable of producing HO_x radicals at night [*Bey et al.*, 1997; *Salisbury et al.*, 2001]. The most important ones are the reactions of alkenes with ozone [e.g., *Paulson et al.*, 1999; *Ariya et al.*, 2000; *Fenske et al.*, 2000; *Siese et al.*, 2001] and NO_3 radicals [e.g., *Mihelcic et al.*, 1993; *Carslaw et al.*, 1997; *Atkinson*, 2000].

[4] In the past years a number of ground-based field campaigns have been performed including OH and/or HO_2 radical measurements. Most of these experiments took place in rural or even remote environments: MLOPEX2 (OH, 1991, 1992) on the island of Hawaii [*Atlas and Ridley*, 1996], TOHPE (OH and HO_2, 1993) at a forested site in the Colorado Rocky Mountains [*Mount and Williams*, 1997], POPCORN (OH, 1994) at a rural, agriculturally used area in northeastern Germany [*Plass-Dülmer et al.*, 1998], IZANA (OH and HO_2, 1994) on the Island of Tenerife [*Armending et al.*, 1997; *Fischer et al.*, 1998], WAO (OH, 1995) in the coastal area of Norfolk, UK [*Forberich and Comes*, 1997], EASE (OH and HO_2, 1996) in the marine boundary layer on the west coast of Ireland [*Carslaw et al.*, 1999], AEROBIC (OH and HO_2, 1997) in a mountainous, forested region of northwestern Greece [*Creasey et al.*, 2001], ALBATROSS (OH and HO_2, 1998) in the remote tropical and subtropical Atlantic Ocean [*Brauers et al.*, 2001], and OKIPEX (HO_2, 1998) at Oki Island in the Japan Sea [*Kanaya et al.*, 2000].

[5] The only HO_x data measured in a more polluted environment which exist in the literature to date, were obtained during LAFRE (1993) at a site 55 km downwind from downtown Los Angeles [*George et al.*, 1999]. Both, OH and HO_2 radical concentrations were measured together with many parameters in control of HO_x. Unfortunately, no measurements of the photolysis frequencies were available. Comparison to box-model calculations revealed relatively good agreement for OH and HO_2 during high NO_x pollution episodes while during periods of lower NO_x concentrations the model overestimated the measurements by about 50%.

[6] In order to better understand the fast radical chemistry in polluted air masses the Photochemistry Experiment in BERLIOZ (PHOEBE) was conducted in July/August 1998 as part of the Berliner Ozonexperiment (BERLIOZ). The measurement site was located in a rural area about 50 km NW of the center of Berlin. A comprehensive collection of measurement techniques provided concentration data of different radicals: OH and HO_2 by laser-induced fluorescence (LIF) (this paper), HO_2, ΣRO_2, and NO_3 by matrix isolation electron spin resonance (MIESR) [*Mihelcic et al.*, 2002], HO_2 + RO_2 by radical amplification (CA) [*Volz-Thomas et al.*, 2002b], and NO_3 by differential optical absorption spectroscopy (DOAS) [*Geyer et al.*, 2001]. In addition a variety of trace gases among them O_3 by short-path UV absorption, NO and NO_2 by chemiluminescence, HONO by DOAS, CO by IR absorption, C_2–C_{10} hydrocarbons by in situ GC, HCHO by liquid-phase fluorescence, higher aldehydes and ketones by GC analysis of cartridge samples, H_2O_2 and CH_3OOH by on-line HPLC. Photolysis frequencies were obtained from filter radiometer ($J(NO_2)$ and $J(O^1D)$) and spectroradiometer measurements ($J(NO_2)$, $J(O^1D)$, J(HONO), J(HCHO), $J(CH_3CHO)$, J(HOOH), $J(CH_3OOH)$). For a complete list of measured parameters, see the work of *Volz-Thomas et al.* [2002a]. Due to its completeness this data set provides the opportunity to shed more light on our current understanding of fast radical chemistry in the planetary boundary layer. An overview of radical measurements during BERLIOZ is presented by *Platt et al.* [2002].

[7] In this paper we present OH and HO_2 radical concentrations as well as photolysis frequencies measured during BERLIOZ. An experimental section will be followed by a discussion of the diurnal cycles of the two radicals in terms of simultaneous observations of nitrogen oxide (NO) and the photolysis frequency of O_3 $J(O^1D)$. The dependencies of the radical concentrations on $J(O^1D)$ and NO_x will be investigated and will be compared to results of previous campaigns. The analysis of the different photolytic sources of OH and HO_2 during BERLIOZ is presented by *Alicke et al.* [2002] and the nighttime radical chemistry is investigated by *Geyer et al.* [2002]. The OH and HO_2 measurements are compared to photochemical box-model calculations with the RACM and the MCM models by *Konrad et al.*

[2002] and Mihelcic et al. (submitted manuscript, 2002), respectively.

2. Experiment

2.1. Measurement Site

[8] A widespread meadow close to the small village Pabstthum, which is located about 50 km NW of the center of Berlin (longitude: 12.94°W, latitude: 52.85°N), was chosen as the site to setup the instrumentation for the PHOEBE field experiment. This site provided an unobstructed airflow from the direction of Berlin over several kilometers. In order to minimize any effects the ground might have on the HO_x radical measurements the containers housing the LIF instrument, the DOAS white-cell system to measure HONO, the peroxy and carbonyl and the photolysis measurements were build up on a platform 5 m high. With the instrument inlets extending above the container roofs a measurement height of 9–10 m above ground was obtained. Other, ground-based instruments, which were located directly beside the platform used inlet lines extending to this height in order to ensure that the same air mass was probed by all the measurements. More details concerning the measurement site are given by *Volz-Thomas et al.* [2002a].

2.2. Measurements of OH and HO_2

[9] The measurement of OH concentrations by LIF spectroscopy takes advantage of the strong rovibronic transitions in the $A^2\Sigma^+(v' = 0) \leftarrow X^2\Pi(v'' = 0)$ band of OH near 308 nm. Ambient air is expanded through a nozzle into a low-pressure fluorescence chamber where it is exposed to pulsed radiation from a narrow-bandwidth laser, which is tuned into resonance with one of the absorption lines. Depending on the OH radical concentration in the air sample a small fraction of the radiation is absorbed. The excited OH radicals will either undergo a collision-induced radiationless transition to the electronic ground state or will relax via the emission of a fluorescence photon within the same vibronic transition. The latter process is used to detect the OH radicals by measuring the amount of fluorescence photons emitted. The observed number of photons is proportional to the ambient OH concentration. Known under the acronym FAGE (Fluorescence Assay by Gas Expansion) this technique was pioneered by *Hard et al.* [1984] and is now widely used by different groups [*Brune et al.*, 1995; *Hard et al.*, 1995; *Holland et al.*, 1995; *Creasy et al.*, 1997; *Kanaya et al.*, 2001].

[10] In order to measure HO_2 radical concentrations with this method NO is added to the flow of ambient air downstream of the nozzle to convert HO_2 into OH, which is subsequently detected via its fluorescence signal. Thus this detection scheme yields a composite signal of ambient OH and OH from the HO_2 conversion. Although the conversion efficiency is less than 100% the HO_2 signal is usually much larger than the OH signal due to the much higher ambient HO_2 concentration.

2.2.1. The LIF Instrument

[11] The LIF instrument used in this campaign utilized two detection channels in order to provide simultaneous measurements of OH and HO_2 concentrations. The experimental setup of a previous version of our instrument equipped with only the OH channel has been described in detail elsewhere [*Holland et al.*, 1995, 1998]. Since then some technical improvements have been made to increase the OH detection sensitivity, which will be discussed in the following brief description of our instrument. Ambient air is expanded through a nozzle into a fluorescence chamber kept constant at a low pressure of 1.3 mbar. The orifice diameter of the nozzle has been decreased from 0.75 to 0.4 mm in order to prevent OH radicals from being lost on condensing water vapor in the expanding gas beam, a phenomenon which had significantly reduced the detection sensitivity during the POPCORN field campaign [*Hofzumahaus et al.*, 1996]. The gas beam formed by the expansion is crossed by the laser beam (diameter about 8 mm) at right angles. An assembly of optical filters and lenses mounted perpendicular to the two beams images the fluorescence volume onto the photocathode of a gated photomultiplier tube (PMT), which detects the fluorescence photons emitted by the excited OH radicals. Compared to the previously used instrument an interference filter with a 2.5 times higher transmission (Corion) was mounted. The PMT signals are counted by a gated photon counter and corrected for the contribution of solar stray light entering the fluorescence chamber through the nozzle orifice. The resulting signal is then normalized to the laser power, which is continuously monitored by a photo diode, and stored in the computer.

[12] A second channel has been added to the instrument to measure ambient HO_2 in parallel with OH. The principle of HO_2 detection is based on the fast reaction of HO_2 with NO to yield OH radicals, which are subsequently detected by LIF. Based on the design of the OH fluorescence chamber, the HO_2 cell houses an additional ring nozzle mounted just downstream of the entrance nozzle, which injects a flow of 4.2 sccm pure NO (purified over Ascarite®) into the expanding gas beam. As in the OH cell the laser beam intersects the gas beam at right angles and a time-gated microchannel plate photomultiplier (MCP) is used to detect the OH fluorescence photons. Although this detector is less sensitive than a PMT it has faster gating characteristics allowing for a higher pressure (3.8 mbar) to be used in the cell. Although the signal, which is measured in this channel, accounts for the sum of OH from HO_2 conversion and ambient OH the term "HO_2 channel" will be used in this paper. The data from this channel have of course been corrected for the ambient OH concentration.

[13] A third fluorescence chamber, in which a high concentration of OH radicals is produced by the 185 nm photolysis of water vapor in argon, provides an OH reference signal with an excellent signal-to-noise ratio, which is recorded in parallel with the ambient air signals to ensure the correct setting of the laser wavelength. The 308 nm radiation (typ. 50 mW) is delivered by a narrow-bandwidth (typ. 6 GHz), grating-tuned dye laser (Lambda Physik LPD 3002), which is pumped by a pulsed, high repetition rate (8.5 kHz) copper vapor laser (Oxford Lasers ACL 35).

[14] During BERLIOZ the instrument was set up in a 20 feet long, 8.5 feet high sea container. The laser light was directed into the fluorescence chambers mounted 1.7 m above the roof of the container by a pair of adjustable mirrors. The beam alignment was controlled by two position-sensitive photodiodes.

2.2.2. Calibration

[15] The instrument was calibrated with a laminar flow tube several times throughout the campaign, using the now

widely accepted technique of water vapor photolysis in synthetic air at 185 nm as a source of both OH and HO_2 radicals [e.g., *Aschmutat et al.*, 1994; *Schultz et al.*, 1995; *Hofzumahaus et al.*, 1997; *Mather et al.*, 1997; *Reiner et al.*, 1997; *Tanner et al.*, 1997; *Holland et al.*, 1998; *Creasey et al.*, 2000; *Kanaya et al.*, 2001]. The simultaneous process of ozone generation through the photolysis of molecular oxygen serves as a chemical actinometer to measure the photon flux at 185 nm:

$$H_2O + h\nu \longrightarrow OH + H \quad (13)$$

$$H + O_2 + M \longrightarrow HO_2 + M \quad (14)$$

$$O_2 + h\nu \longrightarrow O + O \quad (15)$$

$$O + O_2 + M \longrightarrow O_3 + M \quad (16)$$

Thus the respective OH and HO_2 concentrations provided at the exit of the flow tube and sampled by the nozzle (index N) can be derived from an ozone concentration, $[O_3]$, which is usually measured in the excess gas passing outside the nozzle (index E),

$$[OH]_N = [HO_2]_N = \frac{[O_3]_N}{2} \cdot \frac{\sigma_{H_2O}}{\sigma_{O_2}} \cdot \frac{[H_2O]}{[O_2]} \quad (17)$$

$$P = \frac{[O_3]_E}{[O_3]_N} \quad (18)$$

where the factor 2 is the quantum efficiency of the ozone production, σ_{H_2O} and σ_{O_2} are the absorption cross sections of water vapor ($(7.1 \pm 0.2) \times 10^{-20}$ cm^2) and oxygen ($(1.28 \pm 0.05) \times 10^{-20}$ cm^2) at 185 nm(both from our own laboratory measurements), and $[H_2O]$ and $[O_2]$ are the water vapor (typ. 1% abs.) and oxygen concentrations in the calibration gas. The profile factor, *P*, was determined experimentally to be 1.78 ± 0.08. This value is about 7% smaller than what has been measured during the POPCORN campaign. Possible reasons are a shorter flow tube utilized in the present setup of the calibration source (50 cm versus 1.5 m during POPCORN) and the smaller nozzle orifice of the LIF instrument (0.4 versus 0.75 mm during POPCORN). In a long flow tube, the laminar gas flow will develop a parabolic velocity profile, while in a shorter tube the velocity profile will be somewhere in-between a plug and a parabolic profile. Since the velocity distribution of the gas determines the ozone distribution in the flow tube, *P* depends on the length of the tube. The size of the nozzle orifice determines the fraction of the total gas flow, which is sampled by the nozzle and therefore the distribution of the ozone between the ''nozzle'' and the ''excess'' channel in equation (18). From laboratory measurements of *P* for different combinations of tubes with nozzles we know that the shorter flow tube was mainly responsible for the smaller value of *P*.

[16] During the calibration measurements the UV light intensity was attenuated using a cuvette filled with N_2O as a filter to reduce OH concentrations to typ. 9×10^7 cm^{-3}. Since the resulting ozone concentrations were far too small to be measured directly, the light intensity was monitored with a combination of a CsI phototube and a 185 nm interference filter (FWHM = 27.5 nm). Additional measurements with N_2 filled into the cuvette were used to simultaneously acquire the phototube signal and the concentration of ozone (typ. 5 ppb). The ratio between these two quantities, which was stable to within 5% during the course of the campaign, was used to obtain the ozone concentration required in equation (18) from the measured radiation signal. A series of measurements with different N_2O concentrations filled into the cuvette was performed to test the linearity of the phototube. The measured signals closely followed Lambert–Beer's law using the literature value of the N_2O absorption cross section at 185 nm.

[17] While the OH detection sensitivity can be obtained directly from the OH concentration provided by the calibration source and the measured LIF signal, the calibration of the HO_2 channel requires the knowledge of two parameters: the detection sensitivity of OH in the presence of NO and the detection sensitivity of HO_2. In order to determine the latter parameter, the calibration source is tuned to yield only HO_2 radicals by adding a small amount of CO (65 ppm) to the synthetic air. This amount of CO is sufficient to quantitatively convert all OH into HO_2 prior to entering the fluorescence chamber. The measured LIF signal directly yields the required HO_2 detection sensitivity. The OH detection sensitivity in the presence of NO can then be obtained from a second calibration run with OH and HO_2 radicals. It turns out that under our experimental conditions the presence of NO reduces the OH detection sensitivity by 3% due to its higher quenching efficiency. The ratio between the HO_2 and OH detection sensitivity was about 0.9 indicating that a large fraction of the HO_2 radicals were converted into OH.

[18] The detection sensitivities in both measurement channels decreased with increasing ambient water vapor concentration due to quenching of the OH fluorescence. The measured sensitivity changes in the OH and HO_2 channels were -7% and -12% per 1% water vapor concentration, respectively and have been taken into account in the data reduction procedure. This water dependence is completely different from what had been observed during POPCORN, where OH losses on water clusters formed in the cold gas expansion caused a significant drop in the detection sensitivity at very low water vapor mixing ratios [*Hofzumahaus et al.*, 1996]. In the present setup of the fluorescence cells this effect is avoided by using a smaller nozzle orifice, which reduces the strong cooling in the region of the gas beam probed by the laser.

[19] Every 1–2 days the laser system needed an alignment to reestablish its output power. Unfortunately, with the present laser system this procedure could lead to changes in the spectral line profile, which is one of the main parameters determining the OH detection sensitivity. Therefore, whenever the laser system was newly aligned, both channels were calibrated before and after this procedure to account for possible changes in the detection sensitivities. The values obtained (quoted per mol cm^{-3}) for the OH channel were $(1.5–2.4) \times 10^{-7}$ cts mW^{-1} s^{-1}, which is about a factor of three higher than during POPCORN, mainly due to the improved interference filter in the optical detection axis. For HO_2 the sensitivity was $(2.6–4.3) \times 10^{-8}$ cts mW^{-1} s^{-1}. While these numbers demonstrate the variability in the OH detection sensitivity caused by laser alignments, its stability in between calibrations (e.g., during ambient air measurements) was much better as was deduced from the stability of the OH reference signal, which was recorded in parallel with the ambient air data. The standard deviation of

the reference signals within each of these measurement periods was found to vary between 2% and 6% (1σ) thus setting an upper limit on possible sensitivity changes not accounted for in the data reduction process.

[20] The calibration of the LIF instrument determines the accuracy of the OH and HO_2 concentration data and contributes to their statistical error. From the numbers quoted above for the absorption cross sections, the profile factor, and the phototube calibration we estimate the accuracy of our data at ±10% (1σ). This estimate is supported by an HO_2 intercomparison between LIF and MIESR measurements, which were obtained simultaneously for 2 days. The correlation coefficient r of the two data sets and the slope of the linear regression were 0.94 and 1.03 ± 0.08, respectively [*Platt et al.*, 2002]. The standard deviation of the OH reference signal discussed above, defined the contribution of the calibration to the precision of the concentration data.

[21] Based on the sensitivity and the background signal statistics the detection limits of both channels were estimated. During the morning and evening hours when radical concentrations as well as solar stray light signals were low, the LIF background signal was solely determined by the incident laser radiation. Typical count rates in the OH channel were 35 cts s^{-1} (about 3.5 times higher than during POPCORN) and 5 cts s^{-1} in the HO_2 channel. The resulting 2σ detection limits for a total measurement time of 80 s (40 s on and off resonance each) were 3.5×10^5 mol OH cm^{-3} and 9×10^5 mol HO_2 cm^{-3}, respectively. In practice, however, the HO_2 detection limit was not better than 1×10^7 mol cm^{-3} due to an interference signal observed in the HO_2 channel (see below).

2.2.3. Interferences

[22] The measurement of ambient OH and HO_2 concentrations by LIF at low pressure may be subject to interferences due to OH or HO_2 generated in the fluorescence chamber in the presence of ozone and water [*Smith and Crosley*, 1990; *Holland et al.*, 1995]. In order to account for this possibility we have made LIF measurements in synthetic air, varying ozone and water vapor mixing ratios and UV laser power between 0 and 80 ppb, 0.76% and 2.12%, and 10 and 50 mW, respectively. In the OH channel we have identified a small OH fluorescence signal, which showed a linear dependence on ozone and laser power but did not change with the water vapor mixing ratio beyond expected quenching by H_2O. The signal observed in the presence of 50 ppb of ozone was equivalent to the signal caused by an ambient OH concentration of $(3.2 \pm 0.8) \times 10^5$ mol cm^{-3}. This nonphotolytical interference signal compares well to the value of $(2.9 \pm 0.9) \times 10^5$ mol cm^{-3}, which was obtained during the POPCORN campaign [*Holland et al.*, 1998].

[23] In the HO_2 channel the addition of NO to the expanding gas beam inside the chamber caused a much larger fluorescence signal to appear in the presence of ozone. Again, linear dependencies on ozone and laser power were observed. This time however, the interference signal itself and its sensitivity toward ozone both were found to decrease with increasing relative humidity. Doubling the NO flow did not change the signal significantly. Based on a set of 145 measurements the HO_2 interference (in 10^6 mol cm^{-3}) could be parameterized in ozone (in ppb) and relative humidity (RH, in %)

$$HO_2 = (9.2 - 0.024 \cdot RH) + (2.3 - 0.023 \cdot rh) \cdot O_3 \qquad (19)$$

with a correlation coefficient of $r = 0.974$. The standard deviation of 5×10^6 mol cm^{-3} defines the 1σ uncertainty of the correction. The signal, which we observed in the presence of 50 ppb of ozone and a relative humidity of 60%, was equivalent to the signal caused by an ambient HO_2 concentration of $(54 \pm 5) \times 10^6$ mol cm^{-3}. While the OH interference was small and close to the detection limit of the instrument, the interference in the HO_2 channel could account for a significant portion of the measured signal. A comparison of the interference correction to the ambient concentration is shown in Figure 1. Both interferences depend on the specific experimental setup such as the geometry of the fluorescence cell, the gas flow through the nozzle orifice, and the design of the optical train. The mechanisms, which are responsible for the generation of the OH and/or HO_2 radicals inside the fluorescence chamber, are yet to be revealed. The OH and HO_2 measurements presented in this paper have been corrected for their interferences using on-site measurements of ozone and relative humidity. For HO_2 in particular, this correction could occasionally lead to negative concentrations of approximately -7×10^6 mol cm^{-3}, which reflect the uncertainty of this correction.

[24] Another source of interferences in the HO_2 channel is a possible cross sensitivity toward RO_2 radicals. As in the case of HO_2 they undergo a fast reaction with NO leading to the corresponding RO radical, which in turn reacts with molecular oxygen to yield HO_2 and an aldehyde. This HO_2 may then be detected after conversion into OH. However, since the RO + O_2 reaction is slow due to the low partial pressure of O_2 in the fluorescence chamber, less than 1% of the RO is expected to be converted into HO_2. In laboratory experiments we have found that for our experimental conditions the detection sensitivity toward CH_3O_2 is about (5 ± 5)% of the corresponding HO_2 value. This number agrees well with the cross sensitivity due to $C_2H_5O_2$, which has been measured by *Kanaya et al.* [2001]. During this campaign RO_2 measurements by MIESR (Mihelcic et al., submitted manuscript, 2002) and CA [*Volz-Thomas et al.*, 2002b] have shown that the concentration of the organic peroxy radicals were similar to what has been measured for HO_2. We therefore expect this interference to be relatively unimportant.

2.3. Measurements of Photolysis Frequencies

[25] The photolysis frequencies $J(O^1D)$ and $J(NO_2)$ were measured continuously using calibrated filter radiometers. In addition, a scanning spectroradiometer measured spectra of the solar actinic flux, from which photolysis frequencies were derived for O_3, NO_2, HCHO, H_2O_2, CH_3OOH, HONO, and CH_3CHO. The radiometers collected the downwelling solar radiation (2π sr) at a height of 10 m above the ground. The contribution of the ground albedo was estimated to be 5% and was added to the measurements.

2.3.1. Spectroradiometer

[26] The actinic flux spectroradiometer and the evaluation of photolysis frequencies from measured solar spectra has been described in detail by *Kraus and Hofzumahaus* [1998] and *Hofzumahaus et al.* [1999] and only a brief summary will be given here. The spectroradiometer consisted of a 2π sr actinic flux entrance optic, a scanning double monochromator (Bentham DTM 300), a photoelectric detection system (EMI 9250 photomultiplier, current measurement mode), and a PC for data acquisition and system control. The entrance

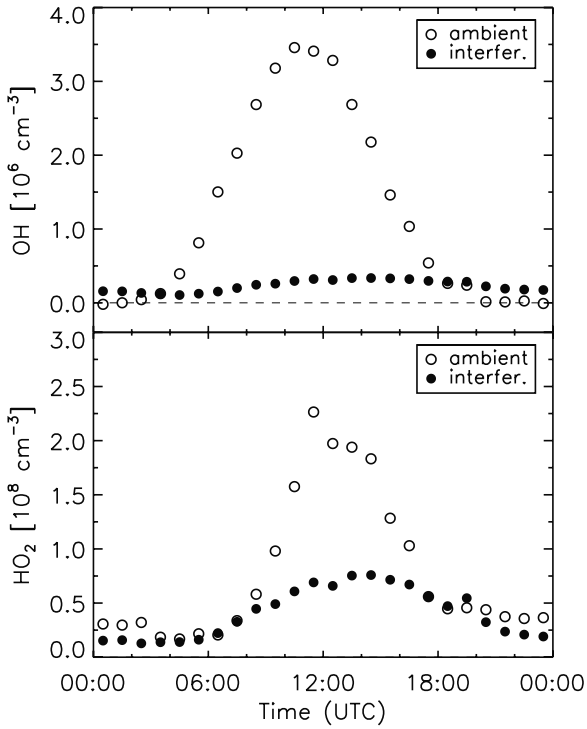

Figure 1. Mean diurnal cycles of the ambient OH and HO_2 measurements (interference corrected) together with the respective interference correction, which was applied to the data. The symbols represent 1-hour averages of all measurements in the respective time-of-day window.

optic was mounted above the LIF container and connected to the monochromator system inside the container by means of a quartz fiber bundle. The spectroradiometer measured actinic flux spectra from 280 nm to 420 nm with a spectral band pass and a stepwidth of 1.0 nm. The measurement time for a spectrum was typically 80 s. The time was accurately synchronized against GPS time. The actinic flux calibration of the spectroradiometer was performed before and after the campaign using certified irradiance standards (FEL 1000 W tungsten–halogen quartz lamps, Gigahertz Optik GmbH, PTB traceable). During the field campaign the calibration was checked periodically using portable transfer standards. The wavelength settings of the monochromator were calibrated against the spectrum of a low-pressure mercury lamp and Fraunhofer lines in the solar spectrum. Photolysis frequencies J were then calculated by numerical integration of the product of the spectral actinic flux $F(\lambda)$, the absorption cross section $\sigma(\lambda)$ and the quantum yield $\phi(\lambda)$ of the respective photodissociation processes:

$$J = \int \sigma(\lambda)\phi(\lambda)F(\lambda)d\lambda \qquad (20)$$

The molecular parameters used for the calculation of the J-values of O_3, NO_2, HCHO, H_2O_2, CH_3OOH, HONO, and CH_3CHO were the same as given by *Kraus and Hofzumahaus* [1998] except for the absorption cross section of NO_2 and the quantum yield of $O(^1D)$, which were given by *Merienne et al.* [1995] and *Talukdar et al.* [1998], respectively. The absolute errors of the J-values are dominated by the uncertainties of the molecular parameters and are estimated to be on the order of ±20% for HCHO, H_2O_2, CH_3OOH, HONO, and CH_3CHO [*Kraus and Hofzumahaus*, 1998]. The total error of $J(O^1D)$ is estimated to be no more than 12%, since the ozone absorption cross section is very well known and the $O(^1D)$ quantum yield has been well established in several new laboratory studies (see overview by *Matsumi et al.* [2002]). The accuracy of $J(NO_2)$ is better than 10% according to an intercomparison (JCOM97) carried out between the spectroradiometer and chemical actinometers in summer 1997 in Jülich [*Kraus et al.*, 2000].

2.3.2. Filter Radiometer

[27] The fixed-bandwidth filter radiometers used for the measurement of $J(O^1D)$ and $J(NO_2)$ were commercial instruments (Meteorologie Consult GmbH) based on the concept by *Junkermann et al.* [1989]. In case of $J(NO_2)$ the instrument included technical modifications of the inlet optic and optical filters as described by *Volz-Thomas et al.* [1996]. The instrument was calibrated against a chemical actinometer during the JCOM97 intercomparison [*Kraus et al.*, 1998]. The error of the calibration is about 7% and uncorrected nonlinearities due to an imperfect spectral response cause an additional error of about ±6%. The comparison with the $J(NO_2)$ measurements by the spectroradiometer in this work shows agreement of the calibrations within 2–3% and is consistent with the results during JCOM97.

[28] The $J(O^1D)$ filter radiometer was similar to the design described by *Junkermann et al.* [1989] but used a modified inlet optic and an additional temperature stabilization of the photodetector assembly. The filter radiometer was characterized in our laboratory with respect to its angular and spectral response. Since the spectral response of the filter radiometer does not match exactly the shape of the ozone photodissociation spectrum, nonlinearities exist between the radiometer signal and $J(O^1D)$, which depend on the solar zenith angle, total ozone column and air temperature. To account for this behavior, a correction function has been derived from a simulation using modeled actinic flux spectra at different solar zenith angles (0°–80°) and different total ozone columns (240–460 DU), and temperatures (270–320 K) [*Müller*, 1994] (B. Bohn, personal communication, 2001). The simulation uses the measured spectral response of the filter radiometer, the temperature dependent ozone absorption cross section by *Malicet et al.* [1995] and the temperature dependent $O(^1D)$ quantum yield by *Talukdar et al.* [1998]. The corrected filter radiometer signals show a good linear correlation against the spectroradiometer measurements, which are used for the absolute calibration of the filter radiometer. The total error of the $J(O^1D)$ values is estimated to be about 13–14% for the conditions of the campaign.

[29] During the BERLIOZ campaign the actinic flux spectroradiometer unfortunately suffered from a malfunction of its computer control, which caused lack of data over extended time periods. In order to fill the data gaps we decided to parameterize the photolysis frequencies of HONO, HCHO (radical and molecular channel), CH_3CHO (radical channel), H_2O_2, and CH_3OOH as a function of the $J(O^1D)$ and $J(NO_2)$ filter radiometer measurements, which are available throughout the campaign. The spectral photodissociation rate coefficients of the two molecules O_3 and NO_2 have a very different wavelength dependence [*Kraus*

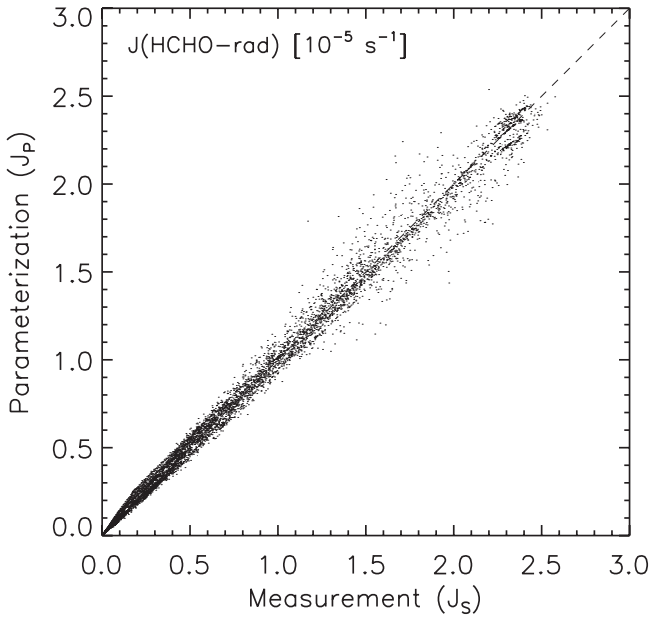

Figure 2. Correlation of the measurement and parameterization of the photolysis frequency of HCHO (radical channel). The dashed line shows the 1:1 relation.

and Hofzumahaus, 1998] and are differently influenced by atmospheric parameters. $J(O^1D)$ is clearly related to the solar UV-B radiation and depends strongly on the solar zenith angle and the total vertical ozone column. In contrast $J(NO_2)$ is a proxy for the UV-A radiation. It does not depend on the atmospheric ozone column and is influenced mostly by the solar zenith angle and atmospheric aerosols. Based on a data set of more than 6000 simultaneous measurements the following function of $J(O^1D)$ and $J(NO_2)$ filter radiometer measurements was used in a weighted multiple linear regression algorithm to fit the spectroradiometer data:

$$J_P(X) = a \times J(NO_2) + b \times J(O^1D) + c \times J(O^1D)^2 \qquad (21)$$

where X denotes one of the molecules listed above. As an example the correlation between the measurement, J_S, and the parameterization, J_P, of J(HCHO, rad. channel) is shown in Figure 2. The other photolysis frequencies exhibit a very similar pattern. The obtained set of coefficients is listed in Table 1. In order to better visualize the deviations between measurements and parameterizations the ratios J_P/J_S of the fits for J(HONO), $J(H_2O_2)$, J(HCHO, rad. channel), and $J(CH_3CHO$, rad. channel) are plotted in Figure 3 as a function of the solar zenith angle. Generally the parameterizations work well for all photolysis channels investigated. Deviations are in the range of ±20% for high solar zenith angles decreasing to less than 10% at local noon. Only in the cases of $J(CH_3CHO)$ and, to a minor extent, J(HCHO) there is a more pronounced systematic deviation from the measurements leading to an overestimation of the photolysis frequency of up to a factor of 2.5 at high solar zenith angles. In all cases the squared correlation coefficient (r^2) was 0.990 or higher. These parameterizations cover a variety of meteorological conditions (χ = 31°–90°, 300–400 DU total ozone, 0–8 octa cloud cover, 6°–28°C ambient temperature) and may be used as input for model calculations dealing with the BERLIOZ data set. Care should be taken, however, when applying these parameterizations to other data sets obtained under different circumstances.

3. The Data

[30] In this section the measurements of ambient air OH and HO_2 radical concentrations and photolysis frequencies will be presented. The discussion will cover the diurnal cycles on the 2 intensive days 20 and 21 July, which are in the focus of the papers in this special section, as well as mean diurnal cycles derived from the complete data set.

3.1. Overview

[31] The LIF measurements cover the time range from 20 July to 6 August 1998. The data set consists of more than 6000 simultaneous measurements of both radicals, among them nine diurnal cycles extending from dawn to dusk with only minor gaps and an extensive set of nocturnal measurements. An overview of OH, HO_2, and selected photolysis frequency measurements obtained during the campaign is shown in Figure 4. Midday OH concentrations ranged from 4×10^6 to 8×10^6 mol cm^{-3}, which is only half of what has been observed during POPCORN [*Holland et al.*, 1998] for similar $J(O^1D)$ and NO_x values. Noon time values of HO_2 varied between 2×10^8 and 4×10^8 mol cm^{-3} with the exception of 21 July when HO_2 concentrations rose to 8×10^8 mol cm^{-3}. At night OH concentrations were usually below the detection limit of our instrument. For HO_2, however, frequently nocturnal concentrations as high as 5×10^7 mol cm^{-3} were observed.

[32] $J(O^1D)$ and $J(NO_2)$ filter radiometer measurements were continuously collected from 16 July to 7 August and from 11 July to 8 August, respectively. The spectroradiom-

Table 1. Coefficients of the Parameterization of Different Photolysis Frequencies Obtained From Spectroradiometer Measurements With Simultaneous Filter Radiometer Measurements of $J(O^1D)$ and $J(NO_2)$[a]

Photolysis frequency	a	b	c	r^{2b}
J(HONO)	0.1492 (4)	15.0 (4)	$-2.4\ (1) \times 10^5$	0.991
$J(H_2O_2)$	$4.43\ (2) \times 10^{-4}$	0.195 (2)	$-2.40\ (6) \times 10^3$	0.993
$J(CH_3OOH)$	$3.22\ (1) \times 10^{-4}$	0.124 (1)	$-1.53\ (4) \times 10^3$	0.993
J(HCHO-rad)	$1.097\ (7) \times 10^{-3}$	0.872 (6)	$-1.03\ (2) \times 10^4$	0.991
J(HCHO-mol)	$2.85\ (1) \times 10^{-3}$	1.00 (1)	$-1.50\ (4) \times 10^4$	0.990
$J(CH_3CHO$-rad)	$5.32\ (8) \times 10^{-5}$	0.1414 (7)	$-9.9\ (3) \times 10^2$	0.993

[a]The 1σ statistical errors are given in parentheses in units of the last figure quoted.
[b]Square of the correlation coefficient between measurement and parameterization.

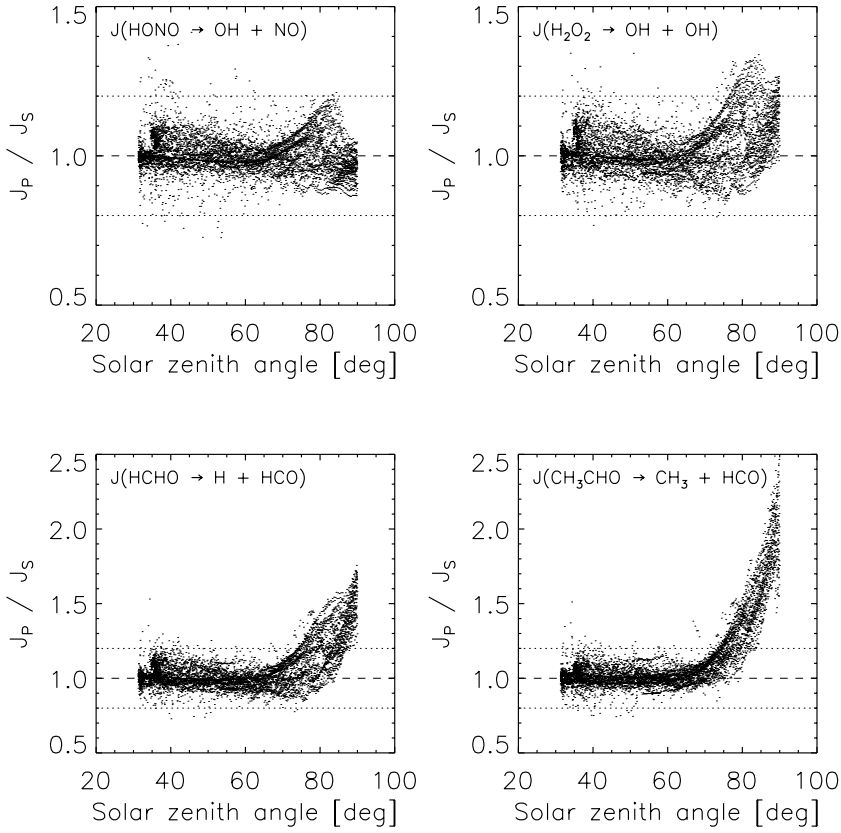

Figure 3. Ratios J(parameterized)/J(measured) for J(HONO), J(H_2O_2), J(HCHO, rad. channel), and J(CH_3CHO, rad. channel) as a function of the solar zenith angle. The dotted lines mark the ±20% range. Note the different ordinate scales in the upper and lower panels.

eter measured seven full diurnal cycles from 16 to 19 July and from 4 to 6 August. Noon time peak values of the ozone photolysis frequency J(O^1D) were highest on the only clear-sky day 20 July reaching 2.5×10^{-5} s^{-1}. While J(O^1D) peak values showed considerable variability throughout the campaign, the nitrogen dioxide photolysis frequency J(NO_2) nearly constantly reached peak values of 0.009 s^{-1}. This can be understood in terms of the higher sensitivity of J(O^1D) toward changes in the ozone column, the ambient temperature, and the aerosol load. The photolysis frequencies of HONO and HCHO (radical channel) are shown as an example for the set of photolysis frequencies, which have been derived from the spectral radiometer measurements. Others, not shown here, include J(NO_2), J(O^1D), J(HCHO, mol. channel), J(acetaldehyde, rad. channel), J(H_2O_2), and J(CH_3OOH).

3.2. Intensive Days 20 and 21 July

[33] The 2 days 20 and 21 July were characterized by a meteorological situation with southeasterly winds during the morning hours, resulting in a transport of polluted air masses from the Berlin city area to the Pabstthum site. Both days were declared as intensive operational periods by the BERLIOZ steering group. Thus, the full set of chemical and meteorological measurements was available during this time. The LIF data set of ambient air HO_x measurements is shown in more detail in Figure 5 together with, J(O^1D) NO, NO_2, and CO measurements. In the following we will discuss these 2 days in some more detail.

3.2.1. 20 July

[34] 20 July was an almost cloud-free day as can be seen from the symmetric and smooth diurnal cycle of J(O^1D). The prevailing wind direction was S-SE, with wind velocities changing from less than 1 m s^{-1} before 0630 UTC, to 3 m s^{-1} around 0700 UTC, more than 6 m s^{-1} around noon and back to 2 m s^{-1} at 1700 UTC. It was the only day during the campaign, where a clear signature of the city plume of Berlin was observed at the Pabstthum site. Vertical soundings of NO_x, O_3, VOCs, and meteorological parameters performed with a tethered balloon system clearly demonstrated the occurrence of a large polluted air mass over the measurement station during the early morning hours [*Glaser et al.*, 2002]. Ground-level measurements of NO_2 and CO between 0800 and 0900 UTC yielded peak values of 12 and 250 ppb,

Figure 4. (opposite) All LIF measurements of ambient air OH and HO_2 radical concentrations obtained throughout the campaign. Photolysis frequency measurements in this time period are shown for J(O^1D) and J(NO_2) (filter radiometer) as well as J(HONO) and J(HCHO, radical channel) (spectroradiometer). Data gaps in the HO_x time series were due to maintenance of the instrument (22, 26, and 30 July and 2 August) and rainy weather (27 July and 2 and 4 August). The data gaps in the spectroradiometer measurements were due to instrument failure. All data are plotted as 5-min averages for the sake of clearness.

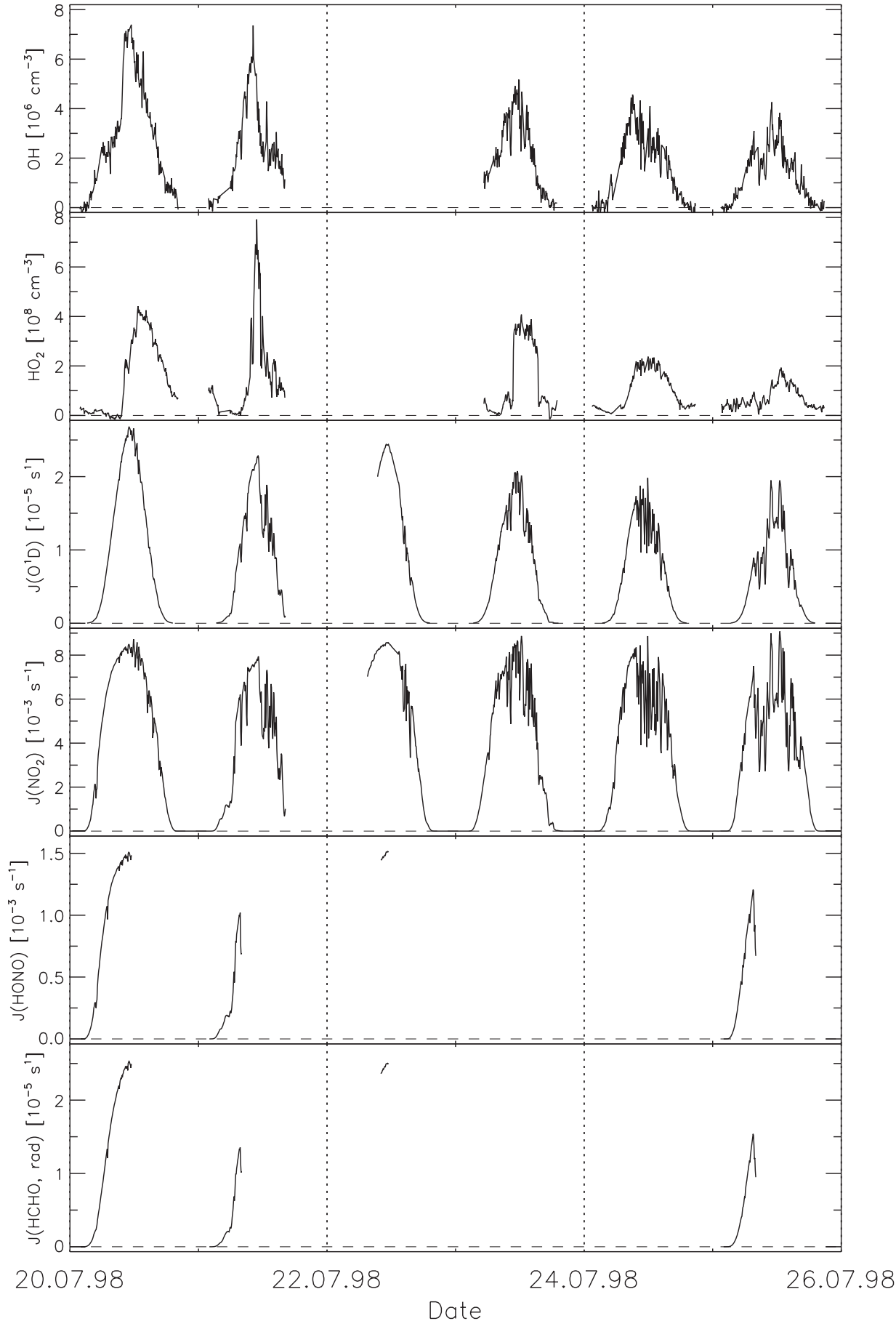
OH [10^6 cm^-3]
HO2 [10^8 cm^-3]
J(O1D) [10^-5 s^-1]
J(NO2) [10^-3 s^-1]
J(HONO) [10^-3 s^-1]
J(HCHO, rad) [10^-5 s^-1]
20.07.98
22.07.98
24.07.98
26.07.98
Date

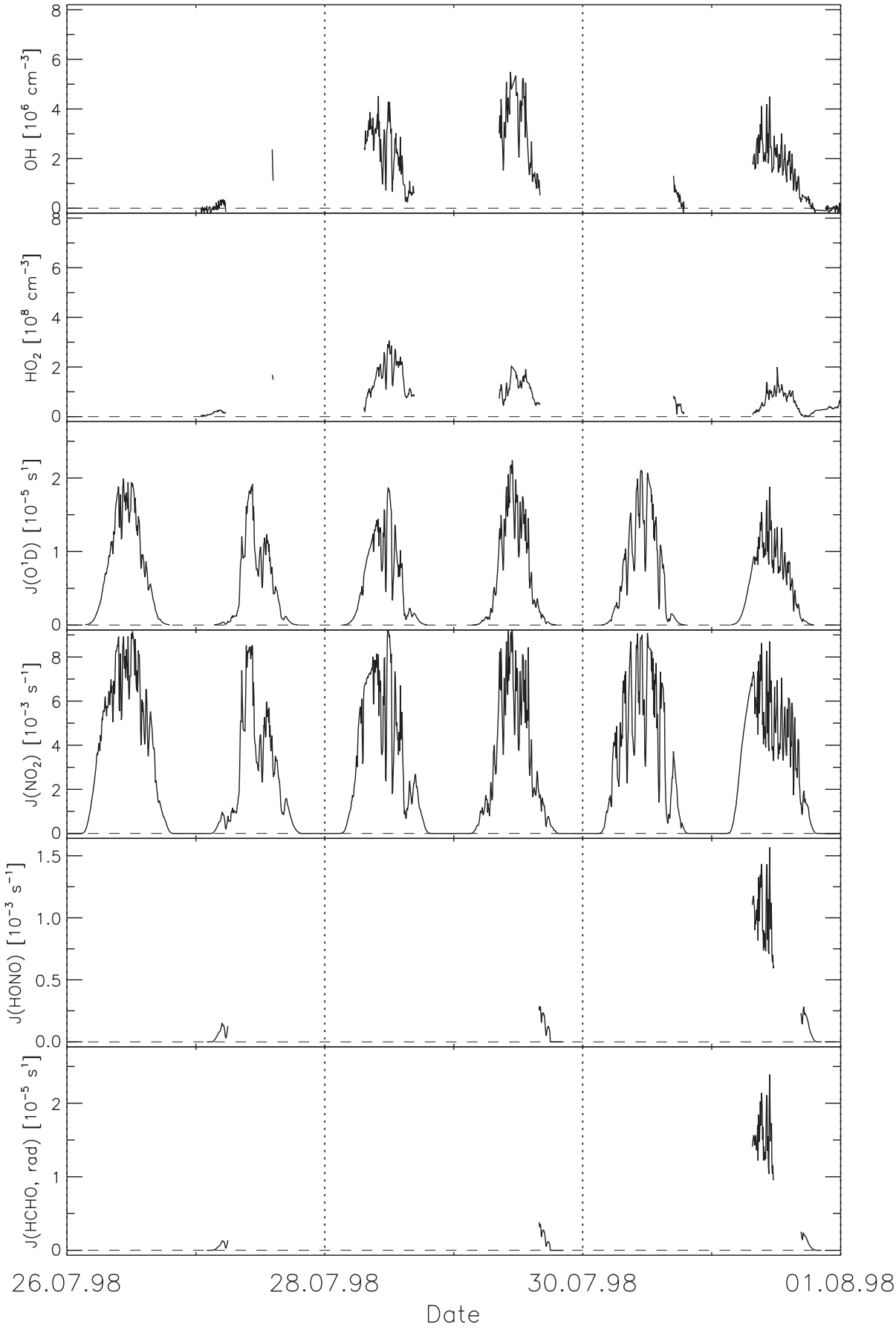

Figure 4. (continued)

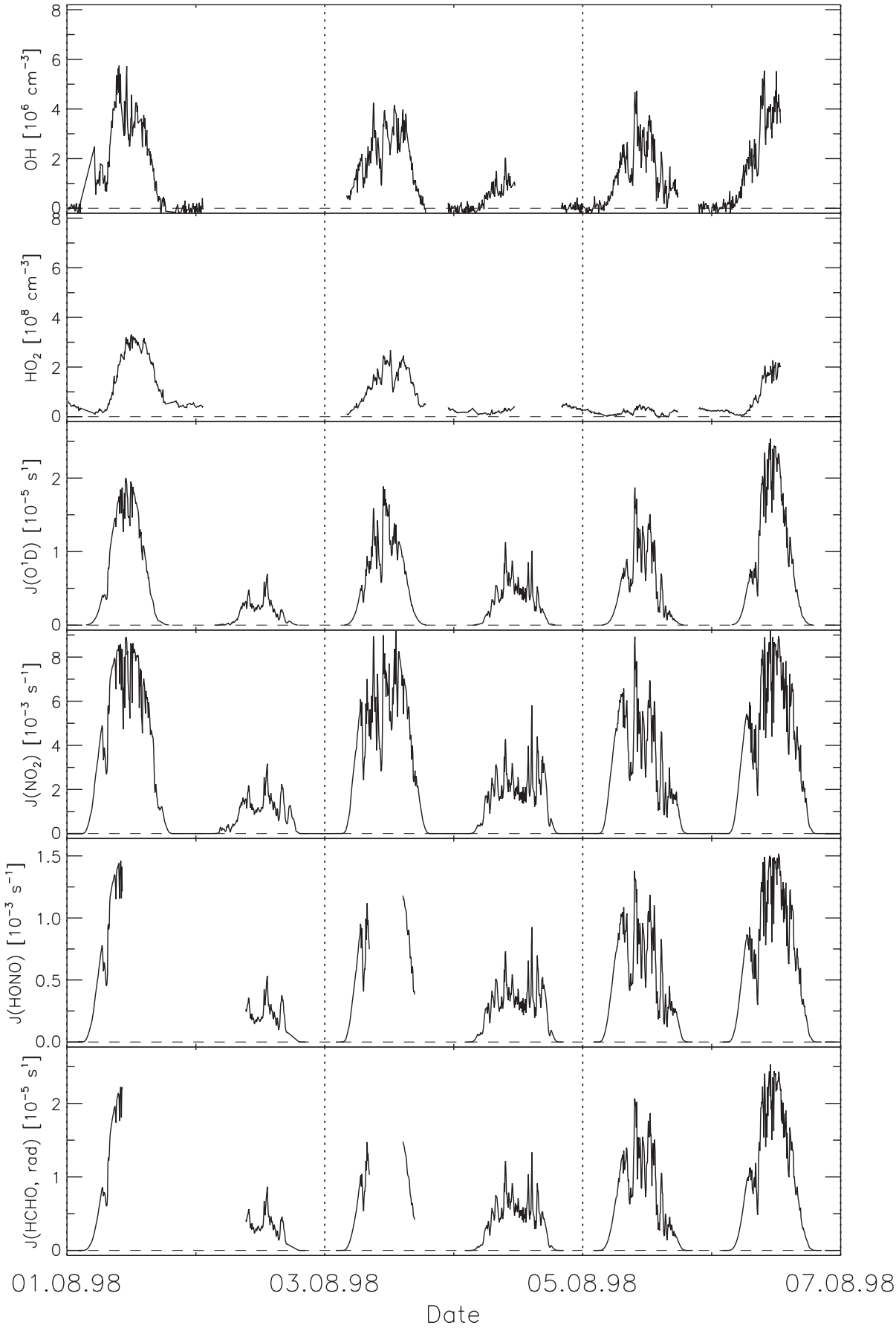

Figure 4. (continued)

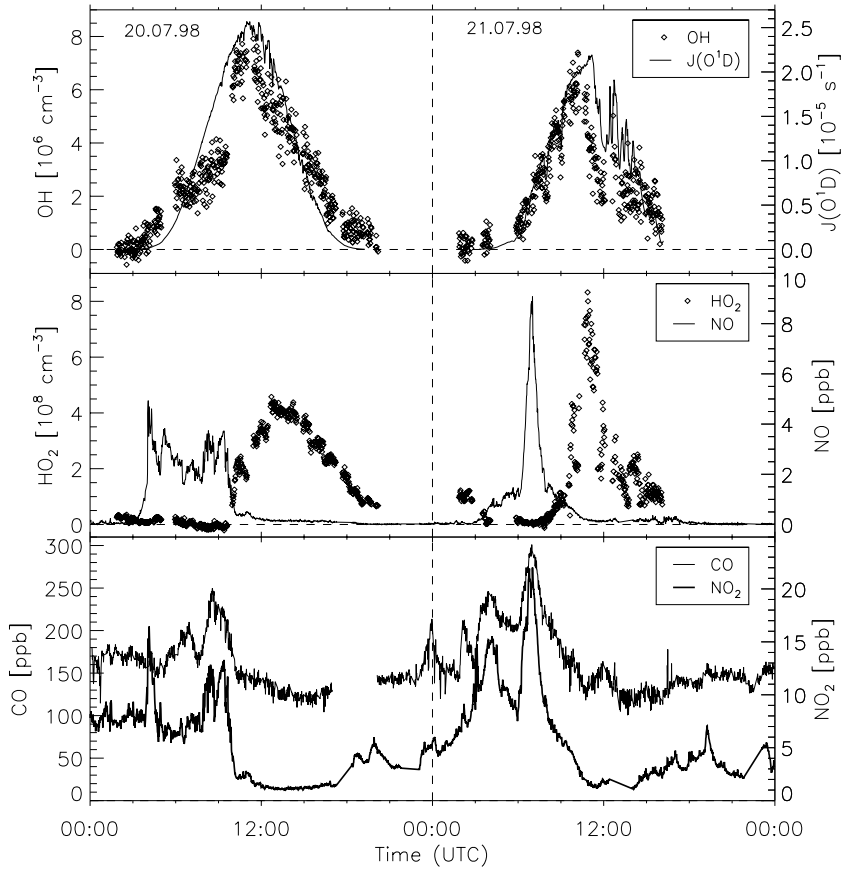

Figure 5. Measurements of OH, HO_2, $J(O^1D)$ (filter radiometer), NO, NO_2, and CO for the 2 intensive days 20 and 21 July.

respectively. Around 0300 UTC NO concentrations started to rise with the onset of the NO_2 photolysis from less than 100 ppt to 5 ppb at 0400 UTC. HO_x measurements started at 0200 UTC that night. While OH concentrations were below the detection limit of our instrument, HO_2 started off at $(2-3) \times 10^7$ cm^{-3} slowly decreasing to concentrations below the detection limit around 0630 UTC, where it remained for the rest of the high pollution episode. OH started to rise at about 0330 UTC, 1 hour earlier than could be expected from OH production due to ozone photolysis. Based on box-model calculations it could be shown that the dominating OH source during these early morning hours was the photolysis of HONO, which showed concentrations of up to 700 ppt that night [*Alicke et al.*, 2002]. Around 0430 UTC the measured OH concentration was 1×10^6 cm^{-3}. At that time the OH production rates from ozone and HONO photolysis were 3×10^4 and 3×10^6 cm^{-3} s^{-1}, respectively. The OH loss was dominated by the reaction with NO_2 yielding a chemical life time of 0.3 s. Between 0600 and 0930 UTC OH concentrations increased from 2.3 to 3.3×10^6 cm^{-3}. This observation is in good agreement with an estimated steady state OH given by $[OH]_{SS} = P_{OH} \cdot \tau_{OH}$, where P_{OH}, the sum of the OH production rates from the photolysis of O_3, HCHO, and HONO, increased from 3.5×10^6 to 7.5×10^6 cm^{-3} s^{-1} and τ_{OH}, the life time of OH with respect to its main loss reaction with NO_2, decreased from 0.6 to 0.4 s.

[35] Between 0930 and 1000 UTC the chemical composition of the air mass changed rapidly toward significantly lower pollution levels due to a change in wind direction, causing the Berlin plume to move away from the measurement site [*Glaser et al.*, 2002]. Measurements of NO_2 and CO around 1030 UTC yielded concentrations of 2.5 and 150 ppb, respectively, steadily decreasing to values as low as 1.3 and 120 ppb around 1500 UTC. Levels of NO first dropped to 400 ppt causing the HO_2 concentration to increase to 2.3×10^7 cm^{-3}. A second drop in NO to less than 200 ppt around 1300 UTC caused HO_2 to nearly double its concentration again. This air mass change was also reflected in the diurnal cycle of OH. Around 0945 UTC its concentration increased from 4×10^6 to 6×10^6 cm^{-3}. The rising concentrations of OH as well as HO_2 can be understood in terms of the still increasing photolytic HO_x production rates and the simultaneously decreasing loss rate mainly due to the lower NO_2 concentration. The diurnal cycles of OH and $J(O^1D)$ both peaked at 1100 UTC while HO_2 reached its maximum concentration approximately 2 hours later. Throughout the afternoon the OH and HO_2 concentrations decreased at a rate slower than the decrease of $J(O^1D)$. During the last hour of measurements that day, e.g., between 1900 and 2000 UTC, we still observed OH and HO_2 concentrations of 6×10^5 and 8×10^7 cm^{-3}, respectively, although $J(O^1D)$ was already zero. While the elevated concentrations of HO_2 can be explained by reactions of hydrocarbons with NO_3 and O_3 [*Mihelcic et al.*, 2002], the OH measurements are underestimated by these model calculations.

3.2.2. 21 July

[36] 21 July was the second intensive day of the campaign. It was characterized by even higher pollution levels during the morning hours than the day before. Around 0700 UTC concentrations of NO_x and CO reached peak values of 30 and 300 ppb, respectively, which were the highest concentrations measured throughout the campaign. This time, however, these elevated concentrations were confined to the lowest 100 m, as could be shown by the vertical NO_x soundings [*Glaser et al.*, 2002], thus excluding the transport process observed the day before as the source of the polluted air mass. Compared to the day before the meteorological conditions were less stable. In the course of the day the wind direction changed from S-SE to NW accompanied by a decrease in wind velocity from 4 to 1 m s^{-1}. Due to varying cloud cover, the photolysis frequencies did exhibit some modulation in particular during the afternoon, when a thunderstorm was approaching.

[37] A first set of HO_x measurements was performed during nighttime between 0200 and 0300 UTC. The average OH concentration in this time window was 1.4×10^5 cm^{-3} with a 1σ error of 5×10^4 cm^{-3}, which was deduced from the precision of the measured count rates, the statistical error of the sensitivity, and the uncertainty of the interference correction. The average HO_2 concentration of $(1.00 \pm 0.02) \times 10^8$ cm^{-3} was well above the detection limit of our instrument. Nighttime chemistry box-model calculations including VOC reactions with NO_3 and O_3 predicted even higher radical concentrations of 4×10^5 and 1.5×10^8 cm^{-3} for OH and HO_2, respectively [*Geyer et al.*, 2002]. The next set of measurements was performed from 0330 to 0410 UTC. The average concentration of OH was $(3.8 \pm 0.7) \times 10^5$ cm^{-3} which compares well to the average OH steady state concentration of $(4.4 \pm 0.8) \times 10^5$ cm^{-3} which was calculated from the HONO photolysis as source of OH and the reaction with NO_2 as OH sink. During the same time period HO_2 concentrations decreased from 4×10^7 cm^{-3} to values below our detection limit. The reason for the decline of HO_2 toward dawn, which was observed on other days as well is less obvious. Assuming that the source of HO_2 is the reaction of NO_3 with VOCs, the HO_2 decrease could be caused by the degradation of NO_3 due to the onset of its photolysis and its reaction with NO. The latter increased in this time period linearly with $J(NO_2)$ from 300 to 700 ppt due to NO_2 photolysis. These NO concentrations were sufficient to limit the lifetime of NO_3 radicals to a few seconds, which is much shorter than what was estimated by *Geyer et al.* [2002] on the basis of VOC reactivities.

[38] Beginning at 0600 UTC OH radical concentrations started to rise linearly with $J(O^1D)$ to reach a maximum concentration of 7×10^6 cm^{-3} at 1015 UTC. HO_2 started to rise at about 0800 UTC, when NO levels had dropped below 1 ppb to reach twice the concentration of the day before. A reason for this high peak value may have been the much higher concentrations of reactive hydrocarbons during noontime on 21 July. While the total measured VOC reactivity toward OH was less than 0.5 s^{-1} on 20 July it increased to 3 s^{-1} the next day mainly due to elevated levels of isoprene, which were a factor of ten higher than the day before [*Konrad et al.*, 2002]. Shortly after 1130 UTC the HO_2 concentration dropped within minutes by a factor of three, a feature that was neither observed for OH, NO, or the photolysis frequencies, nor for any other recorded parameter. This lack of information also became evident in the inability of box-model calculations to reproduce this sharp decrease [*Mihelcic et al.*, 2002]. On that afternoon measurements had to be stopped at 1600 UTC due to an approaching thunderstorm.

3.3. Mean Diurnal Cycles

[39] The main features of the diurnal cycles of OH and HO_2, which have been discussed in some detail for the 2 intensive days 20 and 21 July, were also apparent on the other days of the campaign. The mean diurnal cycles of OH and HO_2 together with $J(O^1D)$, NO, NO_2, and CO averaged over 1-hour time intervals are depicted in Figure 6. We have observed a general good agreement of OH and $J(O^1D)$ during most of the days with deviations in the early morning and late afternoon hours, when $J(O^1D)$ was very small or even zero. At those times the OH production was dominated by other sources as the photolysis of HONO or formaldehyde. With the exception of the night from 20 to 21 July the large data set of nocturnal OH measurements did not yield any evidence for increased nighttime OH levels. The weighted mean of 860 measurements between 2100 and 0300 UTC was $(-2 \pm 8) \times 10^3$ cm^{-3}. The error quotation, however, may be too small since it assumes that the uncertainty of the ozone interference correction, which has been applied to the OH measurements, is of statistical nature only. In order to derive a more conservative upper limit for the mean nighttime OH concentration, we treated this uncertainty as a systematic error contribution. Thus, with a mean nighttime ozone mixing ratio of 25 ± 7 ppb an upper limit of $(4 \pm 1) \times 10^4$ cm^{-3} was estimated for the average nightly OH concentration. Model calculations including VOC reactions with ozone and NO_3 predicted an average nightly OH concentration of $(6 \pm 1) \times 10^4$ cm^{-3} [*Geyer et al.*, 2002].

[40] In the case of HO_2 the dominant dependency on the NO mixing ratio was observed throughout the campaign, a feature, which has been reported for peroxy radicals as well [*Penkett et al.*, 1999]. The mean diurnal cycle of NO was characterized by a pronounced morning peak of 1.2 ppb between 0400 and 1000 UTC, which declined to 200–300 ppt in the afternoon hours and to less then 30 ppt at night. During the early morning hours HO_2 was efficiently suppressed due to its fast reaction with NO. Later on, when the photolysis frequencies strongly increased, HO_2 emerged only slowly, as long as NO levels were high. With decreasing NO, HO_2 concentrations were rising more rapidly to level off between 1100 and 1400 UTC at a maximum concentration of 2×10^8 cm^{-3}. This apparent delay of about 2 hours between the rising slopes of $J(O^1D)$ and HO_2 continued into the afternoon. This behavior is in sharp contrast to the measurements in the marine background atmosphere during ALBATROSS, when a very high correlation of HO_2 and the square root of $J(O^1D)$ was observed [*Hofzumahaus and Webb*, 1998]. Around 1900 UTC, when $J(O^1D)$ was zero, HO_2 concentrations were still as high as 5×10^7 cm^{-3}. Nighttime measurements yielded an average concentration of 3.0×10^7 cm^{-3} with a variability of 1.2×10^7 cm^{-3}. These numbers are in good agreement with model calculations by *Geyer et al.* [2002], who could show that on average the ozonolysis of alkenes and the VOC–NO_3 reactions contributed about equally to the nighttime HO_2 concentration. It is interesting

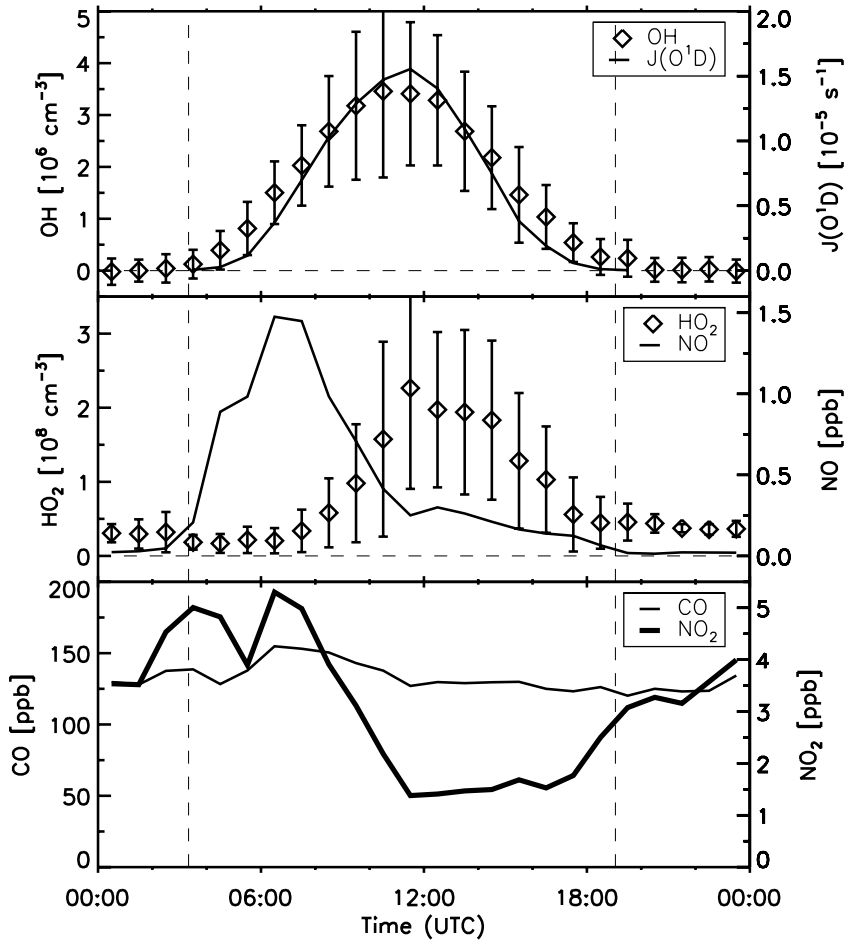

Figure 6. Mean diurnal cycles of OH and $J(O^1D)$ in the upper, HO_2 and NO in the middle, and CO and NO_2 in the bottom panel. The HO_x data shown are 1-hour averages of all measurements in the respective time-of-day window. The ancillary data shown are 1-hour averages of all measurements performed in parallel with the HO_x measurements. The vertical error bars denote the standard deviation of the sample population around the mean. The dashed lines mark the average sunrise and sunset time during the campaign. Local noon was around 1115 UTC.

to notice that although HO_2 concentrations were significantly larger than zero throughout most of the night, this translated into measurable OH only, as long as there was NO available.

[41] Other nighttime HO_2 data have been reported by *Kanaya et al.* [1999] for one night of measurements at Oki Island, Japan. Based on model calculations these authors concluded that the production of the nighttime HO_2 was primarily due to the reaction of ozone with olefins and that NO_3 chemistry was only of minor importance. The production of peroxy radicals at night in the marine boundary layer has been investigated by *Salisbury et al.* [2001]. From their analysis of FAGE and chemical amplifier measurements they deduce that on average the ozone reactions produced twice as many peroxy radicals as the NO_3 reactions.

4. The Correlation of OH and HO_2 With $J(O^1D)$ and NO_x

4.1. $J(O^1D)$ Dependence

4.1.1. OH

[42] The previous discussion has shown that the variability of OH was mainly controlled by changes in the solar UV radiation. In order to quantify this relationship the correlation between OH and $J(O^1D)$ measurements is shown in the upper panel of Figure 7. This correlation does not describe the functional dependency of OH on the photolysis frequency of ozone to O^1D. There are other photolytic reactions, like the photolysis of NO_2 and HCHO, which also influence OH and which are correlated with the photolysis of ozone. Accordingly, $J(O^1D)$ must be considered as a proxy for all those photolytical processes that effect OH [*Ehhalt and Rohrer*, 2000]. On the basis of the whole data set shown in Figure 7, the correlation between the OH data and the $J(O^1D)$ measurements is linear with a correlation coefficient $r = 0.90$. On average, about 81% of the variance of OH can be explained by variations in $J(O^1D)$, which is very similar to what has been observed for the POPCORN data set [*Holland et al.*, 1998]. Part of the variance not accounted for by $J(O^1D)$ is due to the imprecision of the OH measurements themselves, which accounts for about 6% of the total variance. The remaining fraction of 13% subsumes the contributions of all other OH sources and sinks on the OH concentration. Further below we will discuss the variation of OH with NO_x, which can be extracted from the present data set.

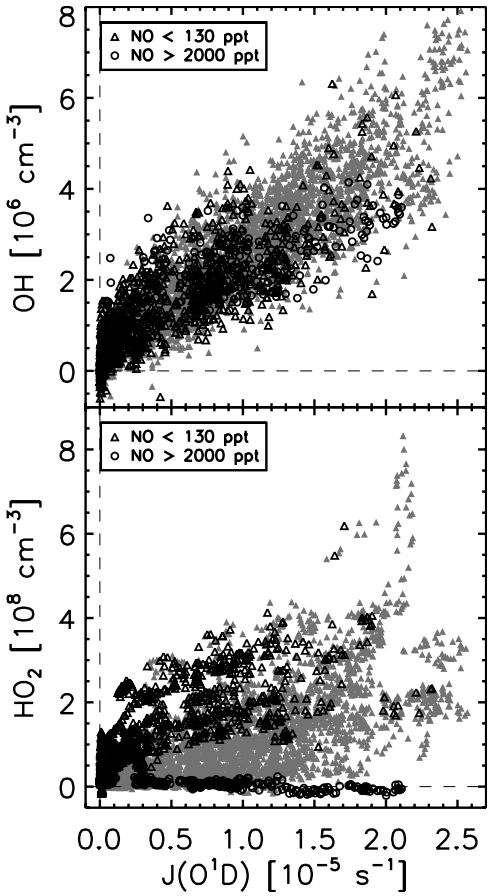

Figure 7. Correlations of $J(O^1D)$ with OH (upper panel) and HO_2 (lower panel). The correlation coefficients, *r*, are 0.90 and 0.60 for OH and HO_2, respectively, both on the basis of the full data set (5024 measurements). Measurements at NO < 130 ppt and NO > 2000 ppt are highlighted as black open triangles and circles, respectively.

[43] A comparison of the measured OH–$J(O^1D)$ dependencies for the three campaigns BERLIOZ, POPCORN, and ALBATROSS is shown in Figure 8. Although we find a high linear correlation between OH and $J(O^1D)$ in all three cases, absolute concentrations of OH for other environments may not simply be deduced from these relationships. Compared to BERLIOZ, measurements during POPCORN yielded OH concentrations, which were nearly twice as large at a given $J(O^1D)$ value, while ALBATROSS OH concentrations [*Brauers et al.*, 2001] were about 30% smaller. In the case of POPCORN lower VOC concentrations at comparable NO_x levels led to higher OH concentrations due to a smaller destruction rate. For ALBATROSS very low NO_x levels efficiently suppressed the secondary OH source from the reaction of HO_2 with NO resulting in smaller OH concentrations.

4.1.2. HO_2

[44] The $J(O^1D)$ dependence of HO_2 is shown in the lower panel of Figure 7. The large variability of HO_2 of more than a decade at a given $J(O^1D)$ value results in a small correlation coefficient of $r = 0.60$. Thus on average only 36% of the total variance of HO_2 can be explained by variations in $J(O^1D)$. In Figure 7 OH as well as HO_2 data, which were measured at NO mixing ratios smaller than 130 ppt or larger than 2 ppb, have been highlighted using different symbols. At high NO, HO_2 is quickly recycled to OH, which is removed by its reaction with NO_2. Thus HO_2 concentrations are small and close to the detection limit of our instrument, independently of the $J(O^1D)$ value. For the case of low NO, recycling of HO_2 to OH becomes less efficient, resulting in higher HO_2 concentrations. At the same time the importance of radical–radical recombination reactions as a sink for HO_x is increasing. Since the sources of HO_2 are dominated by reactions of OH with CO or hydrocarbons, this results in a nonlinear dependence of HO_2 on $J(O^1D)$, which is clearly visible in our data. For OH the $J(O^1D)$ dependence is much less sensitive toward different levels of NO. Only at high $J(O^1D)$ a partitioning of the OH data set into two fractions of different NO concentrations is visible. For a given $J(O^1D)$ value the OH concentrations at high or low NO are lower than at "medium" NO. From this figure it becomes evident that for the present data set OH is strongly determined by $J(O^1D)$ while HO_2 mainly depends on NO. In the following the dependence of OH and HO_2 on NO_x will be discussed in some more detail.

4.2. NO_x Dependence

4.2.1. OH

[45] Qualitatively, OH exhibits a nonlinear dependency on NO_x with a maximum around 1 ppb of NO_x. Toward lower NO_x levels OH concentrations decline due to the decreasing OH production rate from the HO_2 + NO reaction, while the decrease of OH toward higher NO_x can be explained by the increasing importance of the OH loss reaction with NO_2. This nonlinear dependency was predicted by box-model calculations [e.g., *Poppe et al.*, 1993; *Ehhalt*, 1999a] and has been observed in measured data as well [*Eisele et al.*, 1997; *Hausmann et al.*, 1999; *Ehhalt*, 1999a; *Creasy et al.*, 2001].

[46] During BERLIOZ the NO_x mixing ratio varied between 0.3 and 32 ppb. In order to investigate the NO_x dependence, the main source of variance in the OH data, the $J(O^1D)$ dependence, had to be removed. To accomplish this, the data were selected for $J(O^1D) > 7.5 \times 10^{-6}\ s^{-1}$ and each

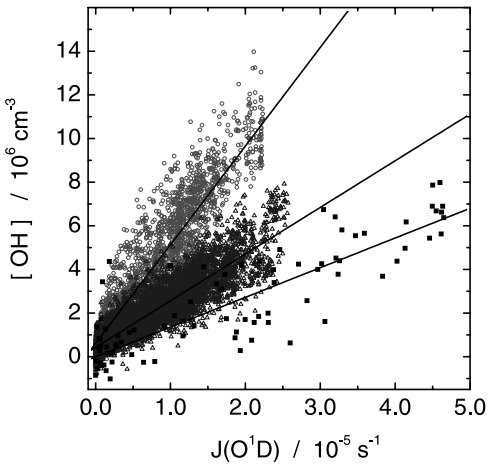

Figure 8. Correlation between OH and $J(O^1D)$ data measured during POPCORN (red circles), ALBATROSS (black squares), and BERLIOZ (blue triangles). See color version of this figure at back of this issue.

OH measurement was normalized to its corresponding $J(O^1D)$ measurement and multiplied by an average $J(O^1D)$ value (1.38×10^{-5} s^{-1}). For further scatter reduction these normalized OH data were averaged over equal log(NO_x, in ppb) intervals of 0.2. The resulting data are shown in the upper panel of Figure 9. The nonlinear dependence is clearly visible. The OH concentration reached a maximum at about 3 ppb NO_x and decreased toward lower and higher NO_x levels as expected. Only for the highest NO_x mixing ratios above 20 ppb the average $J(O^1D)$-normalized OH concentration did not follow the expected dependency, but reached a maximum level of nearly 5×10^6 cm^{-3}. These data have all been measured on 21 July around 0700 UTC. At that time HONO concentrations of 300 ppt have been observed, leading to a photolytic OH production rate of 6×10^6 cm^{-3} s^{-1}, which was about twice as large as what had been contributed by the photolysis of ozone and formaldehyde. Since under these circumstances OH production was not controlled by $J(O^1D)$, normalization of [OH] to $J(O^1D)$ introduces a bias to the data. Presumably, the situation on that day was unique. On 20 July, when NO_x concentrations reached 17 ppb in the time window defined by the $J(O^1D)$ filter, the OH production due to photolysis of HONO was always less than what was obtained from ozone and formaldehyde photolysis. Although no HONO data are available for the other days of HO_x measurements, the significantly lower NO_x concentrations on these days make it unlikely that HONO concentrations increased to sufficiently high levels to dominate the OH production.

[47] In order to see how well the observations can be described by a very basic model, we have calculated steady state OH concentrations for the limiting case of high NO_x using measurements of the different compounds and photolysis frequencies:

$$[\mathrm{OH}]_{SS} = \frac{P_{HO_x}(\mathrm{O_3}, \mathrm{HONO}, \mathrm{HCHO})}{k_{OH+NO_2} \cdot [\mathrm{NO_2}]} \qquad (22)$$

where P_{HO_x} (O_3, HONO, HCHO) is the production rate of OH radicals due to O_3 and HONO photolysis and of HO_2 radicals due to HCHO photolysis. Under high NO_x conditions the latter immediately react with NO to yield OH. The term in the denominator, $k_{OH+NO_2} \cdot [NO_2]$, describes the destruction frequency of OH due to its reaction with NO_2, which is the main HO_x loss reaction in a high NO_x environment. The calculated OH concentrations have been treated the same way as the OH measurements and the resulting data have been incorporated in Figure 9. For high NO_x the approximation is in good agreement with the measurements.

[48] The measured OH–NO_x dependencies for the three campaigns ALBATROSS, POPCORN, and BERLIOZ are compiled in Figure 10. For the ALBATROSS campaign only one data point at very low NO_x is available due to the small natural variability of NO_x in the remote marine background air. As has been discussed above the low OH concentration can be attributed to the missing secondary OH source from the HO_2 + NO reaction. During POPCORN measurements of NO_x ranged from 0.3 to 6 ppb when selected for $J(O^1D) > 7.5 \times 10^{-6}$ s^{-1}. OH concentrations were highest at NO_x mixing ratios between 1 and 2 ppb. For BERLIOZ this maximum was found at a NO_x mixing ratio about 50% higher than during POPCORN, while the OH concentration itself was only half as large as for the previous campaign. An explanation for these observations may be found in the CO and VOC mixing ratios associated with each of the data points, which are not only higher than during POPCORN but also correlated with NO_x [*Konrad et al.*, 2002] as is depicted for CO in Figure 9. With increasing CO and VOC reactivity the OH concentration decreases and the OH maximum is shifted to higher NO_x values as has been discussed by *Poppe et al.* [1993].

4.2.2. HO_2

[49] The diurnal cycles of HO_2 exhibit a strong dependence on the NO_x mixing ratio as became so apparent in Figure 7. As for OH, the relation between HO_2 and NO_x has been investigated in the past using numerous box-model calculations [e.g., *Ehhalt*, 1999a]. Qualitatively, these calculations show the highest HO_2 concentrations at low NO_x. Toward higher NO_x, HO_2 concentrations are predicted to decline first slowly and then more rapidly to finally approach zero. Observations of this dependency have been reported for the upper troposphere [*Brune et al.*, 1999; *Jaegle et al.*, 1999], but are limited to low NO_x levels between 10 ppt and 1 ppb. In order to investigate this relationship in our measurements, the HO_2 data were selected for $J(O^1D) > 7.5 \times 10^{-6}$ s^1 and averaged over equal log(NO_x, in ppb) intervals of 0.2. The measured HO_2–NO_x dependency is shown in the middle panel of Figure 9. Starting from low NO_x mixing ratios the HO_2 concentration increases with increasing NO_x, possibly due to a rising efficiency of the RO_2 + NO + O_2 reaction. HO_2 passes through a maximum at about 1 ppb NO_x, before it starts to decrease toward higher NO_x. This decline approximately follows $1/[NO_x]^2$ due to the conversion of HO_2 into OH with NO and the subsequent HO_x loss reaction of OH with NO_2. This observation was again compared to a very simple approximation of the steady state HO_2 concentration at high NO_x:

$$[\mathrm{HO_2}]_{SS} = \frac{P_{HO_x}(\mathrm{O_3}, \mathrm{HONO}, \mathrm{HCHO})}{k_{OH+NO_2} \cdot [\mathrm{NO_2}]} \cdot \frac{k_{OH+CO} \cdot [\mathrm{CO}]}{k_{HO_2+NO} \cdot [\mathrm{NO}]} \qquad (23)$$

where the first term is the OH steady state concentration as defined above and the second term describes the partitioning of HO_x between HO_2 and OH. These data have been analyzed the same way as the HO_2 measurements and have been added to Figure 9. The observed decline of HO_2 toward higher NO_x mixing ratios is surprisingly well

Figure 9. (opposite) NO_x dependency of measured and calculated OH (upper panel) and HO_2 (middle panel) concentrations and the ozone production rate (bottom panel) derived from the reaction of HO_2 with NO. The data were averaged over equally spaced log(NO_x) intervals. Prior to averaging, the data were selected for $J(O^1D) > 7.5 \times 10^{-6}$ s^{-1}. The OH data have been normalized to $J(O^1D)$ (see text). The symbols and error bars, which mark the mean value and standard deviation of the data in their respective NO_x interval, were positioned at the corresponding average NO_x mixing ratio. Additionally, the average CO mixing ratio in each interval was marked by a circle.

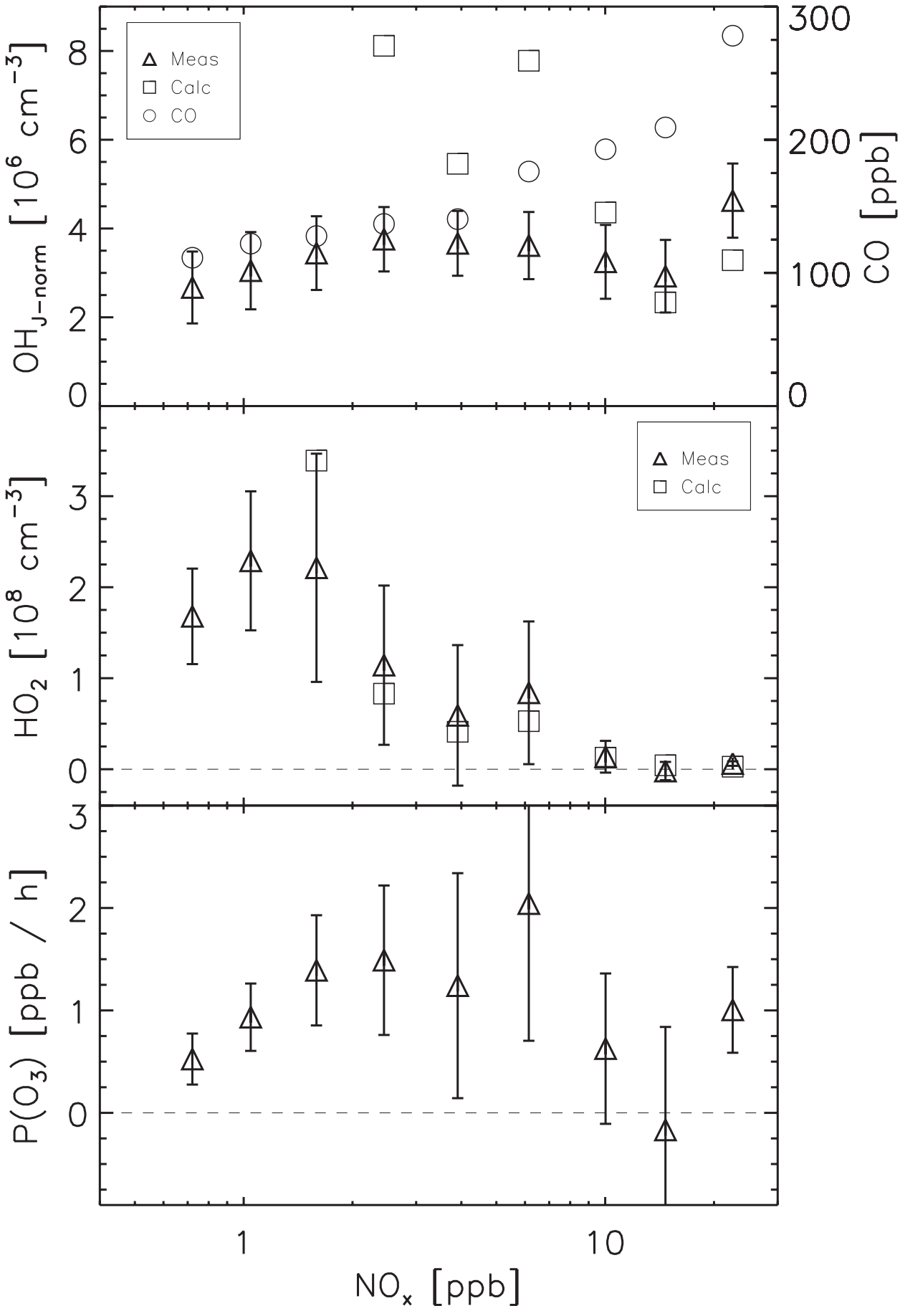
Meas
Calc
CO
OH_{J-norm} [10^6 cm^{-3}]
CO [ppb]
0
2
4
6
8
100
200
300
Meas
Calc
HO_2 [10^8 cm^{-3}]
0
1
2
3
$P(O_3)$ [ppb / h]
0
1
2
3
1
10
NO_x [ppb]

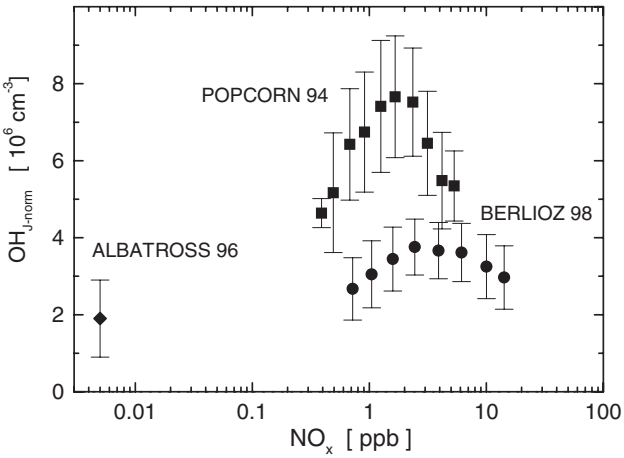

Figure 10. Measured OH–NO_x dependencies for ALBATROSS, POPCORN, and BERLIOZ. The POPCORN and ALBATROSS data were treated the same way as the BERLIOZ data. For details, see the caption of Figure 9.

reproduced by this simple model. It can be regarded as a lower limit since hydrocarbons have been neglected. Including them into the model would add more terms originating from RO_2 + NO reactions to the numerator of the second term in equation (23) thus increasing the HO_2 concentration. The additional loss due to RO_2 + HO_2 reactions is negligible as long as NO_2 concentrations are sufficiently high to determine the overall loss rate in the HO_x system.

[50] Daytime measurements of HO_2 concentrations at Oki Island have been reported by *Kanaga et al.* [2000]. An average noontime value of 2.3×10^8 cm^{-3} has been observed in an environment, which was characterized by high isoprene levels of up to 3 ppb and relatively low ozone and NO_x mixing ratios of less than 30 ppb and 600 ppt, respectively. These data are in agreement with our HO_2 measurements at low NO_x (cf. Figure 9). Similar good agreement was found for measurements of HO_2 at a forested site in Greece, which have been reported by *Creasy et al.* [2001]. They observed an average noontime HO_2 concentration of 2.7×10^8 cm^{-3} for ozone, NO_x, and isoprene mixing ratios of 50, 1, and 1.3 ppb, respectively. A very different situation was found by *George et al.* [1999], who measured OH and HO_2 concentrations during the Los Angeles Free Radical Experiment, which was performed 55 km downwind of downtown Los Angeles. The authors report noontime HO_2 concentrations of 1.5×10^8 cm^{-3} at ozone and NO_x levels around 100 and 25 ppb, respectively. The high HO_2 concentration in the presence of 25 ppb NO_x is very different from our observation, which yielded an average HO_2 concentration below 1.0×10^7 cm^{-3} at NO_x = 22.5 ppb. The very high concentrations of CO, VOC, and aldehydes, which have been measured in the plume of Los Angeles, are certainly necessary to outrun the HO_x loss reaction OH + NO_2, which otherwise would quickly deplete the HO_x reservoir.

4.2.3. O_3 Production

[51] Another parameter which shows a pronounced NO_x dependency is the net ozone production due to the photolysis of NO_2, which has been generated through reactions of NO with HO_2 and RO_2. In order to investigate this relationship we have calculated the NO_2 production rate from the reaction of HO_2 with NO:

$$P_{O_3} \propto P_{NO_2} = k_{HO_2+NO} \cdot [HO_2] \cdot [NO] \quad (24)$$

The NO_x dependence of this parameter is shown in the lower panel of Figure 9. From box-model calculations it is expected that this dependency approximately follows the OH–NO_x relation [e.g., *Ehhalt*, 1999a] which is clearly supported by our data: the ozone production rate due to NO oxidation by HO_2 is low under low and high NO_x conditions and exhibits a maximum between 2 and 3 ppb NO_x. It is interesting to note that the ozone production rate at high NO_x becomes zero as the simple OH steady state approximation approaches the corresponding measurements (cf. upper panel of Figure 9). Where this difference is small, the main loss of OH is via its reaction with NO_2, thus no HO_2 radicals and consequently no ozone are generated. Where the measured OH is smaller than the calculation other sink terms become important, most of which result in the generation of HO_2 and therefore ozone. This observation is a clear indication of the consistency of the measured data sets, which form the basis of the dependencies shown in Figure 9. The apparent enhancement of P_{O_3} at NO_x above 20 ppb is not significant, since the HO_2 data entering equation (24) were at the 1σ detection limit of our instrument. The inclusion of RO_2 radicals into the above expression will increase the total ozone production rate, but is not expected to qualitatively change the observed dependence since at least for 20 and 21 July the RO_2/HO_2 ratio was almost constant during daytime and close to unity (Mihelcic et al., submitted manuscript, 2002). While our measurements clearly show a decreasing ozone production rate with increasing NO_x, observations in the upper troposphere suggest that under conditions of fast convective transport of NO_x together with HO_x precursors P_{O_3} may not always decrease with increasing NO_x [*Jaegle et al.*, 1999].

5. Summary

[52] During the BERLIOZ field campaign in summer 1998 OH and HO_2 radical concentrations as well as photolysis frequencies of different molecules were measured at the rural site Pabstthum about 50 km NW of the center of Berlin. The radical data set includes daytime and nighttime measurements during pollution episodes as well as under clean air conditions over a time period of 18 days. The photolysis frequencies of ozone and NO_2 have been measured continuously using calibrated filter radiometers while the photolysis frequencies of different other molecules, among them HONO and HCHO, were derived from solar actinic flux measurements using a scanning spectroradiometer. Gaps in the latter photolysis frequency time series data were filled with a parameterization in $J(O^1D)$ and $J(NO_2)$ filter radiometer data.

[53] OH radical concentrations rising as high as 8×10^6 cm^{-3} have been observed on 20 July, a day which was

characterized by a rapid change from a polluted to a rural air mass. On average the noon time OH concentration was 3.5×10^6 cm^{-3}, which is only about half of what has been measured during the POPCORN campaign. Nocturnal measurements of OH were usually below the detection limit of our instrument. An upper limit of 5×10^4 cm^{-3} was estimated for the average nightly OH concentration. Generally the daytime OH concentration closely followed the evolution of the diurnal cycle of $J(O^1D)$. During the early morning and late afternoon hours, however, OH concentrations as high as 1.5×10^6 cm^{-3} have been measured at times, when $J(O^1D)$ was basically zero. For the dawn period, the photolysis of HONO, which accumulated during nighttime, proved to be an important source of OH, while after sunset the conversion of HO_2 into OH by reaction with NO may account for the observed OH. The main dependencies of the OH radical concentration have been evaluated. On average about 81% of the variability in OH can be explained by variations in $J(O^1D)$, which serves as a proxy for the photochemically active solar UV radiation. While this is very similar to what has been observed during POPCORN and ALBATROSS, the slope $[OH]/J(O^1D)$ differs significantly for the three campaigns, mainly due to different NO_x and VOC levels encountered during each of these experiments. The NO_x dependency of the OH measurements has been investigated. It exhibits a maximum around 3 ppb NO_x, which is about 50% higher than for the POPCORN data set. This difference again can be attributed to the higher VOC load encountered during BERLIOZ. For high NO_x it was found that the observed dependency could be reproduced with a simple steady state approximation of the OH concentration.

[54] The HO_2 radical concentration reached a maximum of 8×10^8 cm^{-3} on 21 July, a day which was characterized by exceptionally high VOC mixing ratios. On the other days maximum concentrations were only half as high. Unlike OH average nighttime concentrations of HO_2 were 3×10^7 cm^{-3} and thus well above the detection limit of our instrument. While the diurnal cycles of OH most of the time closely followed those of $J(O^1D)$, this dependency on the solar actinic flux and thus on photolytical sources was much less pronounced for HO_2. A parameter with a strong impact on HO_2 was the NO mixing ratio. On many days NO showed a distinct morning peak rising as high as 8 ppb and causing the HO_2 concentration to drop below the detection limit of our instrument. The trigger for the HO_2 concentration to rise again was the decline of NO, which on some days happened very rapidly causing an equally rapid increase of HO_2. This pronounced dependency caused the daytime maximum of HO_2 to occur 1–2 hours past local noon. A closer investigation of the HO_2–NO_x dependency revealed a maximum average HO_2 concentration at NO_x = 1 ppb. The observed HO_2 decline toward higher NO_x mixing ratios was well reproduced by a simple HO_2 steady state approximation. Based on HO_2 and NO measurements an ozone production rate was calculated. Its NO_x dependency is in qualitative agreement with box-model calculations, which predict a very similar dependence for both, OH and P_{O_3}.

[55] In summary, this data set of OH and HO_2 radical concentrations together with the numerous measurements of different trace gas components, photolysis frequencies, and meteorological parameters which have been obtained at Pabstthum sheds more light on our current understanding of fast photochemical processes in polluted as well as rural air masses.

[56] **Acknowledgments.** We wish to thank Michael Sedlacek and Markus Weber who investigated calibration and interference issues of our instrument in laboratory experiments. Further on, we thank Dirk Poppe for helpful discussions on the NO_x dependency of OH and HO_2. Financial support by the BMBF (contract 422-4007 07TFS31/HB.5 and 422-4007 07TFS30/B.2) is gratefully acknowledged.

References

Alicke, B., et al., OH formation by HONO photolysis during the BERLIOZ experiment, *J. Geophys. Res.*, doi:10.1029/2001JD000579, in press, 2002.

Ariya, P. A., R. Sander, and P. J. Crutzen, Significance of HO_x and peroxides production due to alkene ozonolysis during fall and winter: A modeling study, *J. Geophys. Res.*, *105*, 17,721–17,738, 2000.

Armerding, W., et al., Testing the daytime oxidizing capacity of the troposphere: 1994 OH field campaign at the Izana Observatory, Tenerife, *J. Geophys. Res.*, *102*, 10,603–10,611, 1997.

Aschmutat, U., M. Hessling, F. Holland, and A. Hofzumahaus, A tunable source of hydroxyl (OH) and hydroperoxy (HO_2) radicals: In the range between 10^6 and 10^9 cm^{-3}, in *Physico-Chemical Behaviour of Atmospheric Pollutants, Rep. EUR 15,609*, edited by G. Angeletti and G. Restelli, pp. 811–816, Eur. Com., Dir. Gen. XIII, L-2920, Luxembourg, 1994.

Atkinson, R., Atmospheric chemistry of VOCs and NO_x, *Atmos. Environ.*, *34*, 2063–2101, 2000.

Atlas, E. L., and B. A. Ridley, The Mauna Loa observatory photochemistry experiment: Introduction, *J. Geophys. Res.*, *101*, 14,531–14,541, 1996.

Bey, I., B. Aumont, and G. Toupance, The nighttime production of OH radicals in the continental troposphere, *Geophys. Res. Lett.*, *24*, 1067–1070, 1997.

Brauers, T., M. Hausmann, A. Bister, A. Kraus, and H.-P. Dorn, OH radicals in the boundary layer of the Atlantic Ocean, 1, Measurements by long-path laser absorption spectroscopy, *J. Geophys. Res.*, *106*, 7399–7414, 2001.

Brune, W. H., P. S. Stevens, and J. H. Mather, Measuring OH and HO_2 in the troposphere by laser induced fluorescence at low pressure, *J. Atmos. Sci.*, *52*, 3328–3336, 1995.

Brune, W. H., et al., OH and HO_2 chemistry in the North Atlantic free troposphere, *Geophys. Res. Lett.*, *26*, 3077–3080, 1999.

Carslaw, N., L. J. Carpenter, J. M. C. Plane, B. J. Allan, R. A. Burgess, K. C. Clemitshaw, H. Coe, and S. A. Penkett, Simultaneous observations of nitrate and peroxy radicals in the marine boundary layer, *J. Geophys. Res.*, *102*, 18,917–18,933, 1997.

Carslaw, N., D. J. Creasey, D. E. Heard, A. C. Lewis, J. B. McQuaid, M. J. Pilling, P. S. Monks, B. J. Bandy, and S. A. Penkett, Modeling OH, HO_2, and RO_2 radicals in the marine boundary layer, 1, Model construction and comparison with field measurements, *J. Geophys. Res.*, *104*, 30,241–30,255, 1999.

Creasey, D. J., P. A. Halford-Maw, D. E. Heard, M. J. Pilling, and B. J. Whitaker, Implementation and initial deployment of a field instrument for measurement of OH and HO_2 in the troposphere by laser-induced fluorescence, *J. Chem. Soc. Faraday Trans.*, *16*, 2907–2913, 1997.

Creasey, D. J., D. E. Heard, and J. D. Lee, Absorption cross-section measurements of water vapour and oxygen at 185 nm: Implications for the calibration of field instruments to measure OH, HO_2 and RO_2 radicals, *Geophys. Res. Lett.*, *27*, 1651–1654, 2000.

Creasey, D. J., D. E. Heard, and J. D. Lee, OH and HO_2 measurements in a forested region of north-western Greece, *Atmos. Environ.*, *35*, 4713–4724, 2001.

Ehhalt, D. H., Gas phase chemistry of the troposphere, in *Global Aspects of Atmospheric Chemistry, Top. Phys. Chem.*, vol. 6, edited by R. Zellner, pp. 21–110, Steinkopff, Darmstadt, Germany, 1999a.

Ehhalt, D. H., Photooxidation of trace gases in the troposphere, *Phys. Chem. Chem. Phys.*, *1*, 5401–5408, 1999b.

Ehhalt, D. H., and F. Rohrer, Dependence of the OH concentration on solar UV, *J. Geophys. Res.*, *105*, 3565–3571, 2000.

Eisele, F. L., G. H. Mount, D. Tanner, A. Jefferson, R. Shetter, J. W. Harder, and E. J. Williams, Understanding the production and interconversion of the hydroxyl radical during the tropospheric OH photochemistry experiment, *J. Geophys. Res.*, *102*, 6457–6465, 1997.

Fenske, J. D., A. S. Hasson, S. E. Paulson, K. T. Kuwata, A. Ho, and K. N. Houk, The pressure dependence of the OH radical yield from ozone–alkene reactions, *J. Phys. Chem. A*, *104*, 7821–7833, 2000.

Fischer, H., et al., Trace gas measurements during the Oxidizing Capacity of the Tropospheric Atmosphere campaign 1993 Izana, *J. Geophys. Res.*, *103*, 13,505–13,518, 1998.

Forberich, O., and F. J. Comes, Local concentrations of the tropospheric oxidants OH and O_3: Measurement and interpretation, *J. Chem. Soc. Faraday Trans.*, *93*, 2899–2906, 1997.

George, L. A., T. M. Hard, and R. J. O'Brien, Measurement of free radicals OH and HO_2 in Los Angeles smog, *J. Geophys. Res.*, *104*, 11,643–11,655, 1999.

Geyer, A., B. Alicke, S. Konrad, T. Schmitz, J. Stutz, and U. Platt, Chemistry and oxidation capacity of the nitrate radical in the continental boundary layer near Berlin, *J. Geophys. Res.*, *106*, 8013–8025, 2001.

Geyer, A., et al., Nighttime formation of peroxy and hydroxyl radicals during the BERLIOZ campaign: Observations and modeling studies, *J. Geophys. Res.*, doi:10.1029/2001JD000656, in press, 2002.

Glaser, K., U. Vogt, and G. Baumbach, Vertical profiles of O_3, NO_2, NO_x, VOC and meteorological parameters during the BERLIOZ-campaign, *J. Geophys. Res.*, *107*, doi:10.1029/2002JD002475, in press, 2002.

Hard, T. M., R. J. O'Brien, C. Y. Chan, and A. A. Mehrabzadeh, Tropospheric free radical determination by FAGE, *Environ. Sci. Technol.*, *18*, 768–777, 1984.

Hard, T. M., L. A. George, and R. J. O'Brien, FAGE determination of tropospheric HO and HO_2, *J. Atmos. Sci.*, *52*, 3354–3372, 1995.

Hausmann, M., F. Holland, J.-P. Kohlmann, F. Rohrer, and D. H. Ehhalt, Dependence of the OH radical on its precursors: An investigation into the POPCORN results, in *Transport and Chemical Transformation in the Troposphere*, vol. 1, edited by P. M. Borrell and P. Borrell, pp. 382–386, WIT Press, Southampton, UK, 1999.

Hofzumahaus, A., and C. E. Webb, Development of a compact transportable instrument for the measurement of tropospheric OH and HO_2 on remote and airborne platforms (DCHOR), final report for EU project under contract ENV4-CT95-0003, 1998.

Hofzumahaus, A., U. Aschmutat, M. Hessling, F. Holland, and D. Ehhalt, The measurement of tropospheric OH radicals by laser-induced fluorescence spectroscopy during the POPCORN field campaign, *Geophys. Res. Lett.*, *23*, 2541–2544, 1996.

Hofzumahaus, A., et al., Reply on comment by Lanzendorf et al., *Geophys. Res. Lett.*, *24*, 3039–3040, 1997.

Hofzumahaus, A., A. Kraus, and M. Müller, Solar actinic flux spectroradiometry: A technique for measuring photolysis frequencies in the atmosphere, *Appl. Opt.*, *38*, 4443–4460, 1999.

Holland, F., M. Hessling, and A. Hofzumahaus, In-situ measurement of tropospheric OH radicals by laser-induced fluorescence: A description of the KFA instrument, *J. Atmos. Sci.*, *52*, 3393–3401, 1995.

Holland, F., U. Aschmutat, M. Heßling, A. Hofzumahaus, and D. H. Ehhalt, Highly time resolved measurements of OH during POPCORN using laser-induced fluorescence spectroscopy, *J. Atmos. Chem.*, *31*, 205–225, 1998.

Jaegle, L., et al., Ozone production in the upper troposphere and the influence of aircraft during SONEX: Approach of NO_x-saturated conditions, *Geophys. Res. Lett.*, *26*, 3081–3084, 1999.

Junkermann, W., U. Platt, and A. Volz-Thomas, A photoelectric detector for the measurement of photolysis frequencies of ozone and other atmospheric molecules, *J. Atmos. Chem.*, *8*, 203–227, 1989.

Kanaya, Y., Y. Sadanaga, J. Matsumoto, U. K. Sharma, J. Hirokawa, Y. Kajii, and H. Akimoto, Nighttime observation of the HO_2 radical by an LIF instrument at Oki Island, Japan, and its possible origins, *Geophys. Res. Lett.*, *26*, 2179–2182, 1999.

Kanaya, Y., Y. Sadanaga, J. Matsumoto, U. K. Sharma, J. Hirokawa, Y. Kajii, and H. Akimoto, Daytime HO_2 concentrations at Oki Island, Japan, in summer 1998: Comparison between measurement and theory, *J. Geophys. Res.*, *105*, 24,205–24,222, 2000.

Kanaya, Y., Y. Sadanaga, J. Hirokawa, Y. Kajii, and H. Akimoto, Development of a ground-based LIF instrument for measuring HO_x radicals: Instrumentation and calibrations, *J. Atmos. Chem.*, *38*, 73–110, 2001.

Konrad, S., et al., Hydrocarbon measurements at Pabstthum during BERLIOZ and modeling of free radicals, *J. Geophys. Res.*, *107*, doi:10.1029/2002JD000866, in press, 2002.

Kraus, A., and A. Hofzumahaus, Field measurements of atmospheric photolysis frequencies for O_3, NO_2, HCHO, CH_3CHO, H_2O_2 and HONO by UV spectroradiometry, *J. Atmos. Chem.*, *31*, 161–180, 1998.

Kraus, A., T. Brauers, D. Brüning, A. Hofzumahaus, F. Rohrer, N. Houben, H. W. Pätz, and A. Volz-Thomas, Results of the NO_2-photolysis frequency intercomparison JCOM97 (in German), *Reports of Forschungszentrum Jülich ISSN 0944-2952, JUEL 3578*, pp. 14–17, Forsch. Jülich GmbH, Jülich, 1998.

Kraus, A., F. Rohrer, and A. Hofzumahaus, Intercomparison of NO_2 photolysis frequency measurements by actinic flux spectroradiometry and chemical actinometry during JCOM97, *Geophys. Res. Lett.*, *27*, 1115–1118, 2000.

Levy, H., II, Photochemistry of the lower troposphere, *Planet. Space Sci.*, *20*, 919–935, 1972.

Logan, J. A., M. J. Prather, S. C. Wofsy, and M. B. McElroy, Tropospheric chemistry: A global perspective, *J. Geophys. Res.*, *86*, 7210–7254, 1981.

Malicet, J., D. Daumont, J. Charbonnier, C. Parisse, A. Chakir, and J. Brion, Ozone UV spectroscopy, II, Absorption cross sections and temperature dependence, *J. Atmos. Chem.*, *21*, 263–273, 1995.

Mather, J. H., P. S. Stevens, and W. H. Brune, OH and HO_2 measurements using laser-induced fluorescence, *J. Geophys. Res.*, *102*, 6427–6436, 1997.

Matsumi, Y., F. J. Comes, G. Hancock, A. Hofzumahaus, A. J. Hynes, M. Kawasaki, and A. R. Ravishankara, Quantum yields for production of $O(^1D)$ in the ultraviolet photolysis of ozone: Recommendation based on evaluation of laboratory data, *J. Geophys. Res.*, *107*(D3), 4024, doi:10.1029/2001JD000510, 2002.

Merienne, M. F., A. Jenouvrier, and B. Coquart, The NO_2 absorption spectrum, 1, Absorption cross-sections at ambient temperature in the 300–500 nm region, *J. Atmos. Chem.*, *20*, 281–297, 1995.

Mihelcic, D., D. Klemp, P. Müsgen, H. W. Pätz, and A. Volz-Thomas, Simultaneous measurements of peroxy and nitrate radicals at Schauinsland, *J. Atmos. Chem.*, *16*, 313–335, 1993.

Mihelcic, D., F. Holland, A. Hofzumahaus, L. Hoppe, S. Konrad, P. Müsgen, H.-W. Patz, H.-J. Schäfer, J. Schmitz, and A. Volz-Thomas, Peroxy radicals during BERLIOZ at Pabstthum: Measurements, radical budgets, and ozone production, *J. Geophys. Res.*, doi:10.1029/2001JD001014, in press, 2002.

Mount, G. H., and E. J. Williams, An overview of the Tropospheric OH Photochemistry Experiment, Fritz Peak/Idaho Hill, Colorado, fall 1993, *J. Geophys. Res.*, *102*, 6171–6186, 1997.

Müller, M., Messung der aktinischen ultravioletten Strahlung und der Ozon-Photolysefrequenz in der Atmosphäre mittels Filterradiometrie und Spektralradiometrie, Ph.D. thesis, Univ. Bonn, Bonn, Germany, 1994.

Paulson, S. E., M. Y. Chung, and A. S. Hasson, OH radical formation from the gas-phase reaction of ozone with terminal alkenes and the relationship between structure and mechanism, *J. Phys. Chem. A*, *103*, 8125–8138, 1999.

Penkett, S. A., K. C. Clemitshaw, N. H. Savage, R. A. Burgess, L. M. Cardenas, L. J. Carpenter, G. G. McFadyen, and J. N. Cape, Studies of oxidant production at the Weybourne Atmospheric Observatory in summer and winter conditions, *J. Atmos. Chem.*, *33*, 111–128, 1999.

Plass-Dülmer, C., T. Brauers, and J. Rudolph, POPCORN: A field study of photochemistry in north-eastern Germany, *J. Atmos. Chem.*, *31*, 5–31, 1998.

Platt, U., et al., Free radicals and fast photochemistry during BERLIOZ, *J. Atmos. Chem.*, *42*, 359–394, 2002.

Poppe, D., M. Wallasch, and J. Zimmermann, The dependence of the concentration of OH on its precursors under moderately polluted conditions: A model study, *J. Atmos. Chem.*, *16*, 61–78, 1993.

Reiner, T., M. Hanke, and F. Arnold, Atmospheric peroxy radical measurements by ion molecule reaction-mass spectrometry: A novel analytical method using amplifying chemical conversion to sulfuric acid, *J. Geophys. Res.*, *102*, 1311–1326, 1997.

Salisbury, G., et al., Production of peroxy radicals at night via reactions of ozone and the nitrate radical in the marine boundary layer, *J. Geophys. Res.*, *106*, 12,669–12,687, 2001.

Schultz, M., M. Heitlinger, D. Mihelcic, and A. Volz-Thomas, Calibration source for peroxy radicals with built-in actinometry using H_2O and O_3 photolysis at 185 nm, *J. Geophys. Res.*, *100*, 18,811–18,816, 1995.

Siese, M., K. H. Becker, K. J. Brockmann, H. Geiger, A. Hofzumahaus, F. Holland, D. Mihelcic, and K. Wirtz, Direct measurement of OH radicals from ozonolysis of selected alkenes: A EUPHORE simulation chamber study, *Environ. Sci. Technol.*, *35*, 4660–4667, 2001.

Smith, G. P., and D. R. Crosley, A photochemical model of ozone interference effects in laser detection of tropospheric OH, *J. Geophys. Res.*, *95*, 16,427–16,442, 1990.

Talukdar, R. K., C. Longfellow, M. K. Gilles, and A. R. Ravishankara, Quantum yields of $O(^1D)$ in the photolysis of ozone between 289 and 329 nm a function of temperature, *Geophys. Res. Lett.*, *25*, 143–146, 1998.

Tanner, D. J., A. Jefferson, and F. L. Eisele, Selected ion chemical ionization mass spectrometric measurement of OH, *J. Geophys. Res.*, *102*, 6415–6425, 1997.

Volz-Thomas, A., A. Lerner, H. W. Pätz, M. Schultz, D. S. McKenna, R. Schmitt, S. Madronich, and E. P. Röth, Airborne measurements of the photolysis frequency of NO_2, *J. Geophys. Res.*, *101*, 18,613–18,627, 1996.

Volz-Thomas, A., H. Geiss, A. Hofzumahaus, and K.-H. Becker, The Fast Photochemistry Experiment in BERLIOZ (PHOEBE): An introduction, *J. Geophys. Res.*, doi:10.1029/2001JD002029, in press, 2002a.

Volz-Thomas, A., H.-W. Pätz, N. Houben, S. Konrad, D. Mihelcic, P. Müsgen, D. Perner, and T. Klüpfel, Inorganic trace gases and peroxy radicals during BERLIOZ at Pabstthum: An investigation of the photostationary state of NO_x and O_3, *J. Geophys. Res.*, doi:10.1029/2001JD001255, in press, 2002b.

A. Hofzumahaus, F. Holland, and J. Schäfer, Institut für Chemie und Dynamik der Geosphäre II: Troposphäre, Forschungszentrum Jülich, D-52425 Jülich, Germany. (a.hofzumahaus@fz-juelich.de; f.holland@fz-juelich.de)

A. Kraus, Grünenthal GmbH, Zieglerstr. 6, D-52078 Aachen, Germany. (alexander.kraus@grunenthal.de)

H. W. Pätz, ICG 2: Institut für Chemie der Belasteten Atmosphäre, Forschungszentrum Jülich, D-52425 Jülich, Germany. (h.w.paetz@fz-juelich.de)

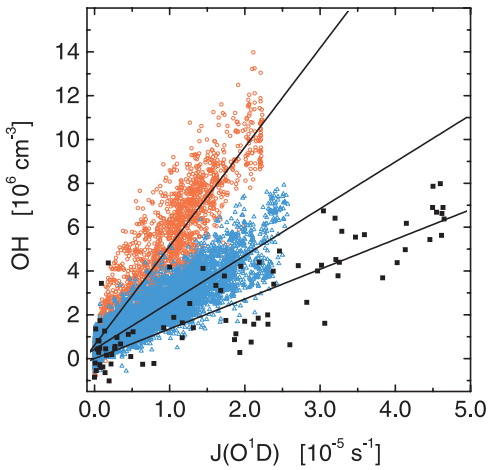

Figure 8. Correlation between OH and $J(O^1D)$ data measured during POPCORN (red circles), ALBATROSS (black squares), and BERLIOZ (blue triangles).